



HAL
open science

The free-fermionic $C^{(1)}_2$ loop model, double dimers and Kashaev's recurrence

Paul Melotti

► **To cite this version:**

Paul Melotti. The free-fermionic $C^{(1)}_2$ loop model, double dimers and Kashaev's recurrence. 2017. hal-01574018

HAL Id: hal-01574018

<https://hal.science/hal-01574018>

Preprint submitted on 9 Nov 2018

HAL is a multi-disciplinary open access archive for the deposit and dissemination of scientific research documents, whether they are published or not. The documents may come from teaching and research institutions in France or abroad, or from public or private research centers.

L'archive ouverte pluridisciplinaire **HAL**, est destinée au dépôt et à la diffusion de documents scientifiques de niveau recherche, publiés ou non, émanant des établissements d'enseignement et de recherche français ou étrangers, des laboratoires publics ou privés.

The free-fermionic $C_2^{(1)}$ loop model, double dimers and Kashaev's recurrence

Paul Melotti*

April 25, 2018

Abstract

We study a two-color loop model known as the $C_2^{(1)}$ loop model. We define a free-fermionic regime for this model, and show that under this assumption it can be transformed into a double dimer model. We then compute its free energy on periodic planar graphs. We also study the star-triangle relation or Yang-Baxter equations of this model, and show that after a proper parametrization they can be summed up into a single relation known as Kashaev's relation. This is enough to identify the solution of Kashaev's relation as the partition function of a $C_2^{(1)}$ loop model with some boundary conditions, thus solving an open question of Kenyon and Pemantle [29] about the combinatorics of Kashaev's relation.

1 Introduction

In 1996 Kashaev introduced a way to rewrite the star triangle transformation of the Ising model [24]. Specifically, let us take a planar graph $G = (V, E)$ with usual coupling constants for the Ising model $(J_e)_{e \in E}$ on the edges. Let us suppose that there is a set of variables g on the vertices and faces of G such that

$$\sinh^2(J_e) = \frac{g_x g_y}{g_u g_v} \quad (1)$$

where x, y are the endpoints of e and u, v are the faces adjacent to e . Then the star-triangle relation, or local Yang-Baxter equation, is equivalent to the variables g satisfying a single polynomial relation:



$$\begin{aligned} & g^2 g_{123}^2 + g_1^2 g_{23}^2 + g_2^2 g_{13}^2 + g_3^2 g_{12}^2 \\ & - 2g_2 g_3 g_{13} g_{12} - 2g_1 g_3 g_{23} g_{12} - 2g_1 g_2 g_{23} g_{13} \\ & - 2g g_{123} (g_1 g_{23} + g_2 g_{13} + g_3 g_{12}) \\ & - 4g g_{12} g_{23} g_{13} - 4g_{123} g_1 g_2 g_3 \\ & = 0. \end{aligned}$$

This relation¹, known as Kashaev's relation, has sparked some interest from the point of view of *spatial recurrences*. It can be embedded in \mathbb{Z}^3 by taking $x \in \mathbb{Z}^3$ and denoting $g = g_x$, $g_i = g_{x+e_i}$, $g_{ij} = g_{x+e_i+e_j}$, etc. Then by choosing the greatest root of a degree 2 polynomial we get [29]:

$$g_{123} = \frac{2g_1 g_2 g_3 + g(g_1 g_{23} + g_2 g_{13} + g_3 g_{12}) + 2XYZ}{g^2}, \quad (2)$$

*Laboratoire de Probabilités, Statistique et Modélisation, Sorbonne Université, campus Pierre et Marie Curie, 4 place Jussieu, F-75005 Paris. Email: paul.melotti@upmc.fr

¹Kashaev's initial equation contained a +4 instead of a -4 coefficient for the last terms, but one can easily get from one to another, for instance by multiplying g by -1 at a vertex of the cube and its three neighbors.

where $X = \sqrt{g_1g_2g_3 + g_2g_3g_1}$, $Y = \sqrt{g_1g_13 + g_1g_3g_1}$, $Z = \sqrt{g_1g_12 + g_1g_2g_1}$.

This transformation (2) is called *Kashaev's recurrence*. It can be iterated to define g on further vertices of \mathbb{Z}^3 , provided we had a sufficiently large set of initial conditions. A remarkable fact is that it exhibits a *Laurentness* phenomenon: the solution of the recurrence at any point is always a Laurent polynomial in the initial variables. This fact is related to cluster algebras [17, 18], but it also hints at a possible hidden object represented by the solution.

Let us quickly review the current state of spatial recurrences: Speyer related the solution of the octahedron recurrence (which can be traced back to Dodgson [12]) to the partition function of a dimer model [35]; then Carroll and Speyer showed that the cube recurrence (proposed by Propp [34]) corresponds to cube groves [5]; more recently Kenyon and Pemantle studied a generalization of Kashaev's relation, known as the hexahedron recurrence, and identified its solution with a double dimer model [29]. Unfortunately, when specialized to Kashaev's recurrence, their model does not provide a one-to-one correspondence between configurations and monomials of the Laurent polynomial. In this paper we provide a model that does give a one-to-one correspondence, known in the physics literature as the $C_2^{(1)}$ loop model.

The $C_2^{(1)}$ loop model was introduced by Warnaar and Nienhuis in [36], among other models, as a loop model naturally associated to formal solutions of the Yang-Baxter equation [3, 23]. It was also considered, for different reasons, by Jacobsen and Kondev in [22] as a generalization of the eight-vertex model, and they conjecture a phase diagram for this model.

It is a dense, two-color loop model where same-colored loops cannot intersect. Let us detail this terminology; see also Figure 1 for an example.

- *loop model* means that the configurations are unions of simple curves. In our case, these curves use edges of the dual graph of a bipartite quadrangulation G , and are able to turn inside faces of G .
- *two-color* means that each loop is either red or blue.
- *dense* means that every dual edge of G belongs to a loop.
- finally, *same-colored loops cannot intersect* means that the only allowed crossings are between red and blue; see Figure 2 for all possible local configurations at a face of G .

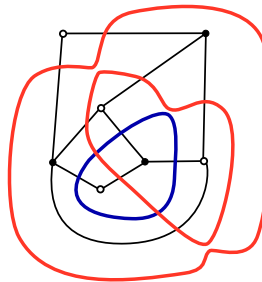


Figure 1: A quadrangulation G (in black), with a $C_2^{(1)}$ loop configuration.

Equivalently, a $C_2^{(1)}$ loop configuration can be seen as a gluing of quadrangles appearing in Figure 2, where only same-colored edges can be glued together.

The model is equipped with weights: let n be a positive parameter called *fugacity*, then the weight of a $C_2^{(1)}$ loop configuration σ is

$$w(\sigma) = n^{\#\text{loops in } \sigma} \prod_{f \in F} w_f^f,$$

where F is the set of faces of the quadrangulation and w_f^f is the local weight corresponding to $\sigma|_f$.

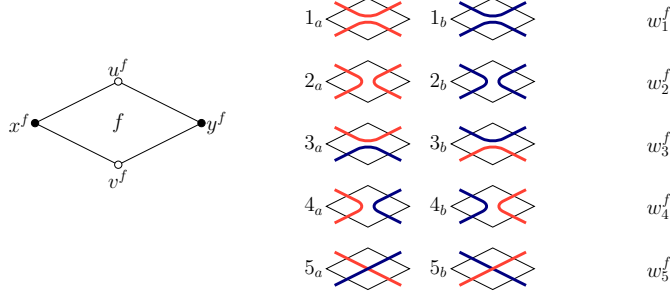


Figure 2: A face f , the 10 local configurations $1_a, \dots, 5_b$ at f and their local weight w_i^f .

In [36] the authors give a two-parameter family of fugacity and weights such that the model is *integrable*, which in their setting means that it satisfies a form of the star-triangle relation:

$$\begin{cases} n = -2 \cos 2\lambda \\ w_1 = \frac{\sin(\lambda-u) \sin(3\lambda-u)}{\sin \lambda \sin 3\lambda} \\ w_2 = -\frac{\sin u \sin(2\lambda-u)}{\sin \lambda \sin 3\lambda} \\ w_3 = \frac{\sin(3\lambda-u)}{\sin 3\lambda} \\ w_4 = -\frac{\sin u}{\sin 3\lambda} \\ w_5 = \frac{\sin u \sin(3\lambda-u)}{\sin \lambda \sin 3\lambda} \end{cases} \quad (3)$$

In [21], Ikhlef and Cardy define a fermionic observable F_s for this model and show that imposing a form of discrete holomorphicity on F_s yields the same integrable weights as in [36]; this approach was extended to the case of non-trivial boundary conditions in [8].

In this paper we only deal with the $n = 2$ case. We introduce the *free-fermionic* relations (see Section 2.3 for more details on this terminology):

$$\begin{aligned} w_1^f w_4^f &= w_3^f w_5^f, \\ w_2^f w_3^f &= w_4^f w_5^f, \\ w_5^f (w_1^f + w_2^f) &= w_3^f w_4^f. \end{aligned}$$

For instance, the integrable weights (3) at $n = 2$ (*i.e.* $\lambda = \pm \frac{\pi}{2}$) satisfy the free-fermionic relations.

When these relations are satisfied, we show that the $C_2^{(1)}$ loop model can be transformed into a double dimer model. We prove the following; for a precise statement, see Theorem 1 of Section 2.

Theorem. *For any free-fermionic $C_2^{(1)}$ loop model, there is a bipartite decorated graph equipped with a dimer model with weights μ , and there are constants $(\lambda_f)_{f \in F}$, such that the partition function \mathcal{Z}_{loop}^G is equal to the square of the partition function $\mathcal{Z}_{dim}(\mu)$ of this dimer model, up to multiplicative factors:*

$$\mathcal{Z}_{loop}^G = \left(\prod_{f \in F} \lambda_f \right) (\mathcal{Z}_{dim}^G(\mu))^2.$$

An application of this result is the computation of the free energy of any free-fermionic $C_2^{(1)}$ loop model on a periodic planar quadrangulation; see Section 2.4.

Then we define a parametrized free-fermionic $C_2^{(1)}$ loop model, analogous to Kashaev's parametrized Ising model (1). Let us suppose that there is a set of variables $(g_v)_{v \in V}$ on the vertices of G such that

$$\begin{cases} w_1^f = g_x g_y \\ w_2^f = g_u g_v \\ w_3^f = \sqrt{g_x g_y} \sqrt{g_x g_y + g_u g_v} \\ w_4^f = \sqrt{g_u g_v} \sqrt{g_x g_y + g_u g_v} \\ w_5^f = \sqrt{g_x g_y g_u g_v}. \end{cases} \quad (4)$$

The existence of such a parametrization is discussed in Appendix B. In particular, we show that it always exists for a free-fermionic model on a lozenge graph.

In this regime, we show that the Yang-Baxter equations associated to the model (corresponding to a move called *cube flip*, similar to the star/triangle move) are equivalent to g satisfying Kashaev's recurrence (2). See Theorem 2 in Section 3.

Finally, we get to the solution of Kashaev's recurrence. See Theorems 3 and 4 of Section 4 for a precise statement of the following.

Theorem. *For any solvable initial condition $(g_i)_{i \in I}$ on $I \subset \mathbb{Z}_-^3$, the solution of Kashaev's recurrence at the origin is*

$$g_{0,0,0} = \sum_{\sigma} \left(2^{\#\text{loops in } \sigma} \prod_f w_i^f \prod_{i \in I} g_i^{-2} \right)$$

where the sum is over taut $C_2^{(1)}$ configurations σ , and the local weights w_i^f are given by (4).

Moreover, there is a one-to-one correspondence between such loop configurations and monomials of $g_{0,0,0}$ as a function of the variables $(g_i)_{i \in I}$.

The *taut* configurations are those satisfying some boundary and connectivity conditions; an example is displayed in Figure 3.

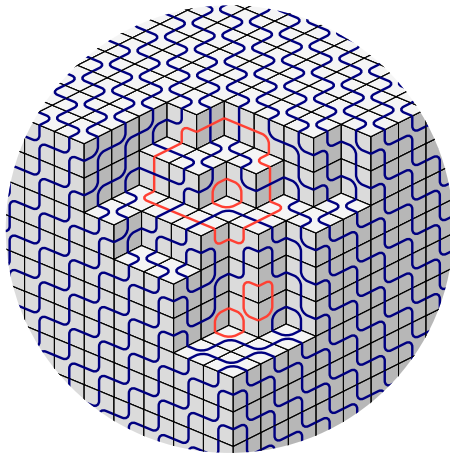


Figure 3: A taut $C_2^{(1)}$ loop configuration.

The paper is organized as follows:

- In Section 2 we define the models, and show how to get from free-fermionic $C_2^{(1)}$ loops to dimers. We also compute the free energy on periodic planar quadrangulations.
- In Section 3 we show that for the parametrization (4) of the weights, the Yang-Baxter equations of loops are equivalent to Kashaev's recurrence.

- In Section 4 we define taut configurations, and prove that the solution of Kashaev’s recurrence is the partition function of these configurations. We compute some limit shapes of the model by a now standard technique [33, 11, 29, 19]. We also show that in characteristic 2 the model reduces to the cube groves of [5].

Acknowledgments

I am very grateful to my Ph.D. advisors Cédric Boutillier and Béatrice de Tilière for the motivations and questions related to the present work, and for their constant help during the writing of this paper. I also thank an anonymous referee for pointing at a mistake in the definition of the free-fermionic regime.

2 Free-fermionic $C_2^{(1)}$ loops and double dimers

2.1 The $C_2^{(1)}$ loop model on a quadrangulation

Definition 1. Let \mathcal{S} be a connected orientable compact surface without boundary. A *quadrangulation* of \mathcal{S} is a finite connected simple graph $G = (V, E)$ embedded in \mathcal{S} so that edges do not intersect, and so that the *faces* of G (the connected components of the complement of the embedding) are homeomorphic to disks and have degree 4. We denote by F the set of faces.

Definition 2. Let G be a bipartite quadrangulation of \mathcal{S} . For every face $f \in F$, we fix names for the vertices of the boundary of f , in clockwise order, as x^f, u^f, y^f, v^f , with x^f, y^f black vertices and u^f, v^f white vertices like in Figure 2. Notice that a vertex will have several names, corresponding to all the faces adjacent to it; we only use these labels to make the 10 different configurations of Figure 2 well defined. When there is no ambiguity, we will also drop the superscript f .

A $C_2^{(1)}$ loop configuration σ on G is the data, for every $f \in F$, of an index $i_k^f \in \{1_a, 1_b, \dots, 5_a, 5_b\}$ (we think of it as $i \in \{1, \dots, 5\}$ and $k \in \{a, b\}$) representing the local configuration $\sigma|_f$, such that glued edges are the same color.

When there is no ambiguity on the face involved, we will often drop the superscript f in i_k^f . Let us denote σ the set $\sigma = \{(f, i_k) \mid f \in F\}$.

Simply stated, a $C_2^{(1)}$ loop configuration on G is an edge-covering set of red or blue loops on the dual graph G^* (which we represent inside a face by turning or crossing when necessary), such that same-colored loops cannot cross.

We equip the faces with a set of positive weights $W = (w_i^f)_{f \in F, i \in \{1, \dots, 5\}}$. For a loop configuration σ we let N_σ be the number of loops in σ . The weight of σ is defined as

$$w_{\text{loop}}^G(\sigma) = 2^{N_\sigma} \prod_{(f, i_k) \in \sigma} w_i^f. \quad (5)$$

The *partition function* of the model is the weighted sum of loop configurations:

$$\mathcal{Z}_{\text{loop}}^G(W) = \sum_{\sigma} w_{\text{loop}}^G(\sigma).$$

2.2 Dimer model on the quad-graph

Let G^* be the dual graph of G . We consider a decorated graph, denoted G^Q , constructed by expanding every vertex of G^* (which has degree 4) into a small quadrangle called a *city*². Cities are connected by edges called *roads*. Let E^Q be the edges of G^Q .

²This terminology is related to the *urban renewal* transformation of the dimer model [30].

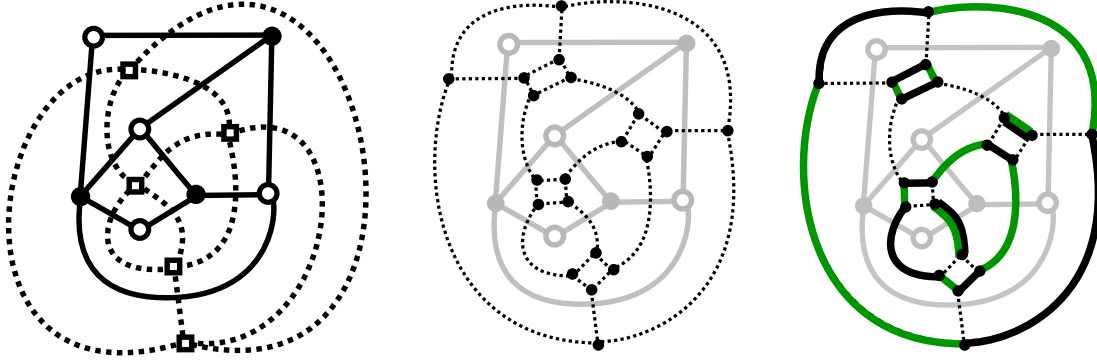


Figure 4: A quadrangulation G of the sphere with its dual G^* (dotted); the decorated graph G^Q (dotted); a double dimer model (m_A, m_B) on G^Q .

A dimer configuration on G^Q is a subset $m \subset E^Q$ such that every vertex of G^Q belongs to exactly one edge of m . Dimer models on G^Q have appeared several times [37, 9, 13, 4] in the study of the 6V model and of the Ising model.

Let $\mu = (\mu_e)_{e \in E^Q}$ be a set of positive real weights on the edges of G^Q . The weight of a dimer configuration is then:

$$w_{\text{dim}}^G(m) = \prod_{e \in m} \mu_e.$$

We similarly define the partition function for dimers:

$$Z_{\text{dim}}^G(\mu) = \sum_m w_{\text{dim}}^G(m),$$

where the sum is over all dimer configurations of G^Q .

The aim of this Section is to provide a direct link between the $C_2^{(1)}$ loop model on G in a certain regime and a couple of independent dimer models on G^Q .

2.3 Free-fermion regime

Let us make the following assumptions on the $C_2^{(1)}$ loops weights (implicitly evaluated at a face $f \in F$), which we call the *free-fermionic relations*:

$$\begin{aligned} w_1 w_4 &= w_3 w_5, \\ w_2 w_3 &= w_4 w_5, \\ w_5(w_1 + w_2) &= w_3 w_4. \end{aligned} \tag{6}$$

Let us make a few remarks on this terminology. We will see that relations (6) are sufficient to transform the $C_2^{(1)}$ loop model into dimers. This idea has been used several times in statistical mechanics to get exact solutions for various models, such as the Ising model [25] and various vertex models [14, 15, 1]. In the physics literature, this technique is sometimes called the ‘‘Pfaffian method’’, since the dimer model’s partition function corresponds to Pfaffians [25]. An alternative representation of Pfaffians is to use Grassman integrals, which are integrals of anti-commuting variables; see for instance [10], chapter 2.B. These anti-commuting variables are interpreted physically as a system non-interacting fermions [20]. This is why any regime for which there is a transformation to dimers is often called *free-fermionic*.

Lemma 1. Let $w_1, w_2, w_3, w_4, w_5 \in (0, \infty)$ be five positive real numbers. Then they satisfy (6) iff there exists a unique triplet $\lambda, a, b \in (0, \infty)$ such that $a^2 + b^2 = 1$ and

$$\begin{cases} w_1 = \lambda a^2 \\ w_2 = \lambda b^2 \\ w_3 = \lambda a \\ w_4 = \lambda b \\ w_5 = \lambda ab. \end{cases} \quad (7)$$

Proof. Given a set of weights $w_1, w_2, w_3, w_4, w_5 \in (0, \infty)$ that satisfy (6), then there is only one candidate for λ, a, b :

$$\begin{aligned} \lambda &= w_1 + w_2, \\ a &= \frac{w_3}{\lambda}, \\ b &= \frac{w_4}{\lambda}. \end{aligned}$$

Then the third equation of (6) simplifies into

$$w_5 = \lambda ab$$

and the first two equations become, respectively

$$\begin{aligned} w_1 &= \lambda a^2, \\ w_2 &= \lambda b^2 \end{aligned}$$

and since $\lambda = w_1 + w_2$, we also have $a^2 + b^2 = 1$ so that the parameterization (7) is correct. Reciprocally, it is easy to check that (7) implies (6). \square

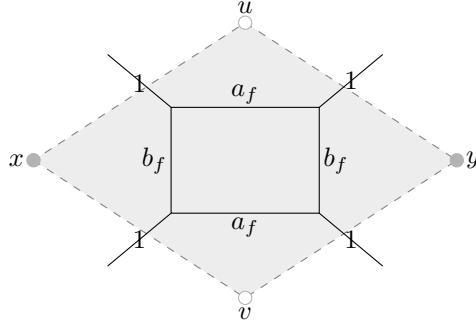


Figure 5: Edge weights for the dimer model on G^Q at a face $f \in F$.

Theorem 1. Let us consider a symmetric $C_2^{(1)}$ loop model such that the free-fermionic relations (6) are satisfied at each face $f \in F$. Let λ_f, a_f, b_f be the corresponding parameters in representation (7).

Let us consider the dimer model on G^Q with weights $\mu = (\mu_e)_{e \in E^Q}$ given by Figure 5.

Then

$$\mathcal{Z}_{loop}^G(W) = \left(\prod_{f \in F} \lambda_f \right) (\mathcal{Z}_{dim}^G(\mu))^2. \quad (8)$$

Proof. **Step 1: double dimers and face weights**

Let us consider a couple of independent dimer configurations m_A and m_B . Dimers A will be colored in black and dimers B in green. Clearly,

$$\left(\mathcal{Z}_{\text{dim}}^G(\mu)\right)^2 = \sum_{m_A, m_B} w_{\text{dim}}^G(m_A) w_{\text{dim}}^G(m_B).$$

Since the roads weights are all equal to 1, the weight of a couple (m_A, m_B) can be seen as a product of “face weight” of the following form; the notation d.dim is a shorthand for “double dimers”:

$$w_{\text{d.dim}}^f(m_A, m_B) := \prod_{e \in m_A \text{ in city } f} \mu_e \prod_{e \in m_B \text{ in city } f} \mu_e. \quad (9)$$

Thus,

$$w_{\text{dim}}^G(m_A) w_{\text{dim}}^G(m_B) = \prod_{f \in F} w_{\text{d.dim}}^f(m_A, m_B).$$

In Figure 6, in the first column, we have listed all local configurations of (m_A, m_B) at a face (up to symmetries).

Step 2: fused double-dimers

In Figure 6, the different rows correspond to the possible occupations of roads by double dimers, and how these roads are connected inside the city (up to symmetries). We can group together the local configurations belonging to the same row, to get a *fused* double dimer configuration. More precisely, a fused dimer configuration $\overline{(m_A, m_B)}$ is the equivalence class of the couples of dimer configurations (m_A, m_B) having identical roads, and having the same connections of single-dimered roads.

We can define face weights for fused dimers, simply by summing the double dimers’ face weights; they are given in the third column of Figure 6. We denote these local weights by $w_{\text{f.d.dim}}^f(\overline{(m_A, m_B)})$, and the weight of a fused double dimer configuration is simply

$$w_{\text{f.d.dim}}^G(\overline{(m_A, m_B)}) = \prod_{f \in F} w_{\text{f.d.dim}}^f(\overline{(m_A, m_B)}).$$

We thus get a weight-preserving (many-to-one) mapping between a couple of dimer models and a fused dimer model. We represent such a mapping by a diagram:

$$\text{Dimers}_A \times \text{Dimers}_B \longrightarrow \text{Fused dimers.}$$

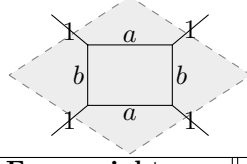
Step 3: marked loops

Let us now focus on the $C_2^{(1)}$ loops part. We define a *marked* $C_2^{(1)}$ loop configuration as a $C_2^{(1)}$ loop configuration where every red edge is marked with an index 0 or 2, and every blue edge with an index A or B , so that the index on a path stays constant except when a different-colored path is crossed. When a different-colored path is crossed, the index has to change.

To make this definition well defined, we need the following Lemma:

Lemma 2. *When G is a connected bipartite quadrangulation on a connected orientable surface, for every $C_2^{(1)}$ loop configuration σ on G , every blue loop of σ crosses red paths an even number of times (and similarly for red loops).*

Proof. Let us color the vertices of G in black and white. Let us consider a blue loop of σ , and let us chose an orientation for that loop. When the loop turns right or left inside a face, the color of the vertex on its left does not change. On the other hand, when the loop goes straight into a face (*i.e.* when it crosses a red loop), this color changes. Since the surface is orientable, when we follow the loop from start to end, we end up with the initial vertex on its left. Therefore it has crossed red paths an even number of times. \square



Dimers m_A, m_B	Fused dimers (m_A, m_B)	Face weight $\sum w_{\text{d.dim}}^f(m_A, m_B)$ $= w_{\text{f.d.dim}}^f((m_A, m_B))$	Marked loops σ^m	Face weight $w_{i_{\sigma^m}(f)}^f$	
		a^2		λa^2	*
		a^2		λa^2	*
		1		$\lambda a^2 + \lambda b^2$ $= \lambda$	
		$a^4 + b^4 + 2a^2b^2$ $= 1$		$\lambda a^2 + \lambda b^2$ $= \lambda$	
		b^2		λb^2	*
		b		λb	*
		$a^2b + b^3$ $= b$		λb	*
		ab		λab	*

Figure 6: Local configurations at a face for double dimers, fused dimers and marked loops. For each row marked with a *, similar rows could be obtained by applying a symmetry or by switching the role of dimers A and B .

For a marked loop configuration σ^m , let σ be its unmarked version. The weight of σ^m is defined just as in (5), except there is no factor for the number of loops; we use the notation m.loop for marked loops:

$$w_{\text{m.loop}}^G(\sigma^m) = \prod_{(f, i_k) \in \sigma} w_i^f. \quad (10)$$

Since there are 2^{N_σ} ways to mark a $C_2^{(1)}$ loop configuration σ , the sum of all possible marked loop weights is equal to the weight of σ . Therefore there is a weight-preserving (2^{N_σ} -to-one) mapping:

$$\text{Marked } C_2^{(1)} \text{ loops} \longrightarrow C_2^{(1)} \text{ loops.}$$

Step 4: marked loops to fused dimers

Let us describe a mapping from marked loops to fused double dimers. Given a marked loop configuration σ^m , let us first put dimers on roads: put one A dimer on blue roads marked with an A , one B dimer on

blue roads marked with a B , two dimers on red roads marked with a 2 , and no dimer on red roads marked with a 0 . Then, let us chose the dimers in cities: when four blue edges come together at a face, chose the city dimers according to the loops connections (see the first row of Figure 6). Otherwise, there is only one possible fused dimer configuration with roads constructed as before. We thus construct a fused double dimer configuration (m_A, m_B) . All the cases (up to symmetries) are listed in Figure 6.

This transformation is several-to-one, indeed, loop configurations having four red loops marked with a 2 (resp. a 0) are mapped onto the same fused dimer configuration. However, up to a global multiplicative factor λ , this transformation is weight-preserving because, after summing over marked loops having the same image, the local weights of both models differ by a same factor λ .

Thus there is a weight-preserving (many-to-one) mapping:

$$\text{marked } C_2^{(1)} \text{ loops} \longrightarrow \text{Fused dimers.}$$

Step 5: conclusion

To sum things up, there is a series of (many-to-one) weight-preserving mappings:

$$\text{Dimers}_A \times \text{Dimers}_B \longrightarrow \text{Fused dimers} \longleftarrow \text{Marked } C_2^{(1)} \text{ loops} \longrightarrow C_2^{(1)} \text{ loops.}$$

This implies the equality of partition functions, which concludes the proof of Theorem 1. \square

From there, it is natural to ask what information between dimers and loops is kept through these transformations. At the local level, it seems that the best connection we can get is the following:

Given a $C_2^{(1)}$ loop configuration σ , let σ_b be the set of blue paths in σ . If a particular set of blue paths σ_b^0 is fixed, we say that a double dimer configuration (m_A, m_B) has paths σ_b^0 if its set of single-dimer roads is the set of blue edges in σ_b^0 , and when the four incoming edges at a city are blue, the dimers in the city are with connection according to σ_b^0 . Then we have:

$$\sum_{\substack{\sigma \text{ } C_2^{(1)} \text{ loops conf.} \\ \text{s.t. } \sigma_b = \sigma_b^0}} w_{\text{loop}}^G(\sigma) = \sum_{\substack{(m_A, m_B) \text{ dimers conf.} \\ \text{with paths } \sigma_b^0}} w_{\text{dim}}^G(m_A) w_{\text{dim}}^G(m_B). \quad (11)$$

As a result, all the observables of the $C_2^{(1)}$ loop model related to blue loops and their connectivity correspond to some observable of the double dimer model, which can in turn be computed by determinantal techniques [26]. On the other hand, the connectivity of red loops seems to be lost in translation. Of course, since red and blue loops play a symmetric role, the statistics of red loops connectivities are the same as the blue loops' and can be computed in the same way; what we actually mean is that the joint connectivities of red and blue loops may not be analyzed through the dimer model.

Example. Probability of a dimer on a road.

Let $e \in E^Q$ be a road in G^Q . We are interested in the probability p of that road being covered by a dimer in a single dimer model m_A , with our previous dimers weights. So

$$p = \mathbb{P}_{\text{dim}}(e \in m_A) = \frac{\sum_{m_A | e \in m_A} w_{\text{dim}}^G(m_A)}{\mathcal{Z}_{\text{dim}}^G}.$$

When we take two independent dimer models m_A, m_B , the probability of e being covered by a single dimer is then $2p(1-p)$. Because of the relation with loops, this is equal to the probability of e being covered by a blue loop. Since loops are color-symmetric, this is equal to $\frac{1}{2}$, and we deduce that

$$p = \frac{1}{2}.$$

This is true for any dimer model on a G^Q with roads having weight 1 and cities having weights a, b such that $a^2 + b^2 = 1$. This property can be proven straightaway studying this dimer model, but is trivial in loops.

Remark 1. *We have presented the correspondence with dimers on a quadrangulation without boundary, but it is possible to consider, for instance, finite quadrangulations of the plane with a boundary. In that case, there is a number of external dual edges (which we think of as “half-edges”, not connected together to the external face), and we have to chose boundary conditions for the $C_2^{(1)}$ loop model. For instance, we could use free boundary conditions by imposing nothing on the red or blue paths that use these external edges; we could also impose the colors of these paths to be fixed; we could even specify how paths starting on external edges are connected inside the graph.*

The equivalence with dimers works similarly by defining appropriate boundary conditions for dimers, except if the specification for loops connections concern both blue and red connections, since we cannot keep track of both colors’ connections in our mappings.

One example of tractable boundary conditions, where only blue connections are specified, will be studied in Section 4.

2.4 Free energy

In this paragraph, we consider an infinite quadrangulation G of the plane \mathbb{R}^2 (so it is necessarily bipartite), that is \mathbb{Z}^2 -periodic. This means that there is a basis (e_x, e_y) of \mathbb{R}^2 such that the translations by e_x and e_y are color-preserving graph isomorphisms.

We define a toroidal exhaustion of G in the following way: for any $n \in \mathbb{N}^*$, G_n is the quotient of G by the lattice $n\mathbb{Z}e_x + n\mathbb{Z}e_y$. We note V_n, E_n, F_n its set of vertices, edges and faces. For each n , G_n is a bipartite quadrangulation on the torus. The graph G_1 is called the *fundamental domain* of our quadrangulation G .

We assume that every face f of G_1 is equipped with a set of weights w_1^f, \dots, w_5^f that satisfy the free-fermion relations (6). Then we can define a $C_2^{(1)}$ loop model on G_1 using these weights. We extend those weights periodically to get a similar model on G_n : every face f of G_n has a unique representative f_0 in G_1 and inherits the weights of f_0 .

We will use the shorthand notation \mathcal{Z}_n for the partition function $\mathcal{Z}_{\text{loop}}^{G_n}(W)$ of this loop model on G_n . Our goal is to compute the *free energy* of this model, which we define without a minus sign following [7, 28]:

$$\mathcal{F} = \lim_{n \rightarrow \infty} \frac{1}{n^2} \log \mathcal{Z}_n.$$

The fact that this limit exists and its exact value will follow from the correspondence with dimers.

We consider the dimer model of Theorem 1 for the fundamental domain G_1 . It can be extended periodically to get a dimer model on G_n . We simply note μ this set of dimers weights. Then by Theorem 1,

$$w\mathcal{Z}_n = \left(\prod_{f \in F_1} \lambda_f \right)^{n^2} \left(\mathcal{Z}_{\text{dim}}^{G_n}(\mu) \right)^2$$

so that

$$\frac{1}{n^2} \log \mathcal{Z}_n = \sum_{f \in F_1} \log(\lambda_f) + \frac{2}{n^2} \log \left(\mathcal{Z}_{\text{dim}}^{G_n}(\mu) \right). \quad (12)$$

The right-hand side of (12) contains the free energy of the periodic dimer model on G^Q with weights μ . This quantity can be exactly computed [7, 28]. Let us recall how this computation is made.

The graph G_1^Q , is a bipartite graph on the torus. We equip it with a Kasteleyn orientation (*i.e.* an orientation of edges such that every face has an odd number of clockwise edges; there exists such an orientation,

see for instance [6]). We can split its vertices between black ones B_1^Q and white ones W_1^Q . Then we define its Kasteleyn matrix K_1 as a W_1^Q by B_1^Q weighted adjacency matrix, with entries

$$(K_1)_{w,b} = \begin{cases} \mu(e) & \text{when } \begin{array}{c} w \xrightarrow{e} b \\ \circ \quad \bullet \end{array} \\ -\mu(e) & \text{when } \begin{array}{c} w \xleftarrow{e} b \\ \circ \quad \bullet \end{array} \\ 0 & \text{otherwise.} \end{cases}$$

Let z and w be two complex numbers. We construct a modified matrix $K_1(z, w)$ in the following way. Let γ_x, γ_y be the two oriented cycles on the torus corresponding respectively to e_x, e_y . We multiply the weight of edges crossing γ_x by z when the white vertex is on the left of γ_x , and by z^{-1} when the white vertex is on the right of γ_x ; and similarly for γ_y and w . These weights define a Kasteleyn matrix $K_1(z, w)$. The *characteristic polynomial* of G_1 is then:

$$P(z, w) = \det K_1(z, w).$$

The free energy of the dimer model can be expressed using the characteristic polynomial:

Theorem ([7, 28]). *We have*

$$\lim_{n \rightarrow \infty} \frac{1}{n^2} \log \left(\mathcal{Z}_{dim}^{G_n}(\mu) \right) = \frac{1}{(2i\pi)^2} \int_{\mathbb{T}^2} \log |P(z, w)| \frac{dz}{z} \frac{dw}{w}.$$

Therefore, (12) gives

$$\mathcal{F} = \sum_{f \in F_1} \log(\lambda_f) - \frac{1}{2\pi^2} \int_{\mathbb{T}^2} \log |P(z, w)| \frac{dz}{z} \frac{dw}{w}. \quad (13)$$

Example. Free energy for integrable weights on \mathbb{Z}^2 . Let us take for G the quadrangulation \mathbb{Z}^2 . We equip every face with the positive integrable weights of [36, 21] for the fugacity $n = 2$:

$$\begin{cases} w_1 = \sin^2(\theta) \\ w_2 = \cos^2(\theta) \\ w_3 = \sin(\theta) \\ w_4 = \cos(\theta) \\ w_5 = \sin(\theta) \cos(\theta) \end{cases} \quad (14)$$

where $\theta \in (0, \frac{\pi}{2})$. Then for all $f \in F$, $\lambda_f = 1, a_f = \sin(\theta), b_f = \cos(\theta)$.

The corresponding weighted graph G_1^Q , equipped with a Kasteleyn orientation, is represented on the left of Figure 7. We can perform an urban renewal [30] on this graph to get the graph on the right.

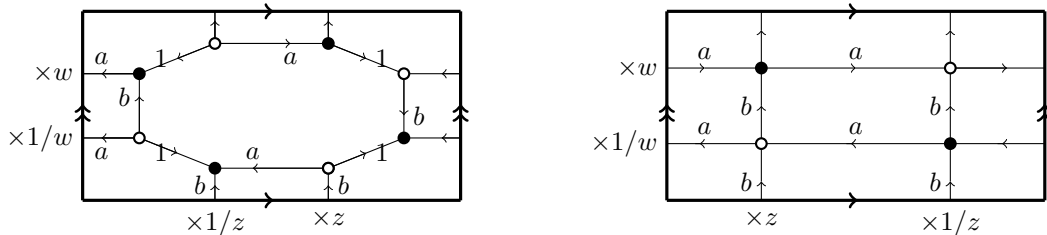


Figure 7: The dimers' fundamental domain G_1^Q , before (left) and after (right) urban renewal, equipped with a Kasteleyn orientation. Here $a = \sin(\theta), b = \cos(\theta)$.

By using the free energy for dominoes on \mathbb{Z}^2 [16] with horizontal weight $\sin(\theta)$ and vertical weight $\cos(\theta)$, we get

$$\mathcal{F} = -\frac{1}{2\pi^2} \int_{\mathbb{T}^2} \log \left| -2 + \cos^2(\theta) \left(z + \frac{1}{z} \right) + \sin^2(\theta) \left(w + \frac{1}{w} \right) \right| \frac{dz}{z} \frac{dw}{w}.$$

Several other expressions can be given for this quantity, for instance following [27]:

$$\mathcal{F} = \frac{2}{\pi} L(\theta) + \frac{2}{\pi} L\left(\frac{\pi}{2} - \theta\right) + \frac{2\theta}{\pi} \ln(\tan(\theta)) + \ln(2 \cos(\theta))$$

where L is the Lobachevsky function.

3 Cube flip and Kashaev's recurrence

From now on, G might be a planar quadrangulation in the sense of Definition 1, or a finite planar quadrangulation with a boundary, in the following sense:

Definition 3. A quadrangulation with a boundary is a finite simple graph $G = (V, E)$, properly embedded in the plane, such that all *internal* (bounded) faces have degree 4.

In this case, we define a $C_2^{(1)}$ loop model on G by specifying a boundary condition in any way discussed in Remark 1 – since the correspondence with dimers won't be used, both blue and red connections can be specified.

We start by proving a few identities on Kashaev's relation, then we relate the star-triangle relation for loops to Kashaev's relation.

3.1 Kashaev's recurrence

Kashaev's relation reads:

$$\begin{aligned} & g^2 g_{123}^2 + g_1^2 g_{23}^2 + g_2^2 g_{13}^2 + g_3^2 g_{12}^2 \\ & - 2g_2 g_3 g_{13} g_{12} - 2g_1 g_3 g_{23} g_{12} - 2g_1 g_2 g_{23} g_{13} \\ & - 2g g_{123} (g_1 g_{23} + g_2 g_{13} + g_3 g_{12}) \\ & - 4g g_{12} g_{23} g_{13} - 4g_{123} g_1 g_2 g_3 = 0. \end{aligned} \tag{15}$$

If seven of the g variables are positive real numbers, then the eighth one can be deduced from (15), up to the choice of the square root of a quadratic polynomial. The choice of the greatest root guarantees that the g variables stay positive. In this case, the recurrence can be explicitly written, see Proposition 1.

We define six other variables X, Y, Z, X_1, Y_2, Z_3 by

$$\begin{aligned} X &= \sqrt{g g_{23} + g_2 g_3}, \\ Y &= \sqrt{g g_{13} + g_1 g_3}, \\ Z &= \sqrt{g g_{12} + g_1 g_2}, \\ X_1 &= \sqrt{g_1 g_{123} + g_{12} g_{13}}, \\ Y_2 &= \sqrt{g_2 g_{123} + g_{12} g_{23}}, \\ Z_3 &= \sqrt{g_3 g_{123} + g_{13} g_{23}}. \end{aligned} \tag{16}$$

All of these quantities can be nicely represented on the vertices and faces of a cube, see Figure 8.

The following relations can be obtained by simple calculations:

Proposition 1 (Kashaev's recurrence). *When Kashaev's relation (15) is satisfied, the value of g_{123} obtained by taking the greatest root reads*

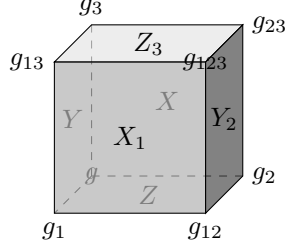


Figure 8: The g , X , Y and Z variables, implicitly taken at $x \in \mathbb{Z}^3$.

$$1. \quad g_{123} = \frac{2g_1 g_2 g_3 + g(g_1 g_{23} + g_2 g_{13} + g_3 g_{12}) + 2XYZ}{g^2}.$$

Furthermore,

$$2. \quad X_1 = \frac{g_1 X + YZ}{g},$$

$$3. \quad Y_2 = \frac{g_2 Y + XZ}{g},$$

$$4. \quad Z_3 = \frac{g_3 Z + XY}{g},$$

$$5. \quad \frac{X_1 Y_2 Z_3 + g_{12} g_{13} g_{23}}{g_{123}} = \frac{XYZ + g_1 g_2 g_3}{g}.$$

The first 4 relations are a particular case of the *hexahedron recurrence* [29].

Kashaev's relation (15) has the same symmetries as the cube. In particular, by considering the central symmetry relative to the center of the cube, we get that the previous transformation is self-dual, in the following sense:

Proposition 2. *Let g_{123} be defined in terms of $g, g_1, g_2, g_3, g_{12}, g_{13}, g_{23}$ as in Item 1 of Proposition 1. Then the transformation:*

$$\begin{pmatrix} g \\ g_1 \\ g_2 \\ g_3 \\ g_{23} \\ g_{13} \\ g_{12} \end{pmatrix} \mapsto \begin{pmatrix} g_{123} \\ g_{23} \\ g_{13} \\ g_{12} \\ g_1 \\ g_2 \\ g_3 \end{pmatrix}.$$

is an involution.

Also note that this involution exchanges X and X_1 , Y and Y_2 , Z and Z_3 .

3.2 Parametrization of a free-fermionic $C_2^{(1)}$ loop model

Let us suppose that there is a set of positive real values on the vertices V of G , denoted $g = (g_x)_{x \in V}$, such that the local loop weights take the following form at a face $f = x \begin{smallmatrix} u \\ \diamond \\ v \end{smallmatrix} y$:

$$\left\{ \begin{array}{ll} \begin{array}{c} \text{Diagram 1} \\ \text{Diagram 2} \\ \text{Diagram 3} \\ \text{Diagram 4} \\ \text{Diagram 5} \end{array} & \begin{array}{l} w_1^f = g_x g_y \\ w_2^f = g_u g_v \\ w_3^f = \sqrt{g_x g_y} \sqrt{g_x g_y + g_u g_v} \\ w_4^f = \sqrt{g_v g_u} \sqrt{g_x g_y + g_u g_v} \\ w_5^f = \sqrt{g_x g_y g_u g_v} \end{array} \end{array} \right. \quad (17)$$

Notice that these weights satisfy the free-fermionic relations (6). In fact, on a class of planar quadrangulations that includes finite lozenge graphs (embedded graphs whose internal faces are non-degenerate rhombi with same edge length), every free-fermionic $C_2^{(1)}$ loop model can be parametrized in this way. This is proved in Appendix B.

Notice also that the bipartite coloring of G is no longer important to define the weights. We will no longer show this coloring.

We can define a marked model with these weights using the weights of equation (10). We will show that the Yang-Baxter equations for this marked loop model are equivalent to g satisfying Kashaev's relation. This implies a similar statement for non-marked loops as well as for the double dimer model. However, since the indices on loops don't affect the weight, the proof for marked loops will not be any more difficult than what it would be for non-marked loops.

We now denote by $\mathcal{Z}_{\text{m.loop}}^G(g)$ the partition function of marked loops on G :

$$\mathcal{Z}_{\text{m.loop}}^G(g) = \sum_{\sigma} w_{\text{m.loop}}^G(\sigma)$$

where σ runs over all marked $C_2^{(1)}$ loop configurations on G , and $w_{\text{m.loop}}^G(\sigma)$ is the same as (10) with the local weights defined by (17).

3.3 Cube flip

Let us suppose that G contains a vertex $x \in V$ of degree 3, such that the graph around x looks like the left-hand side of Figure 9. We can perform a ‘‘cube flip’’ at x by changing the edges around this vertex. It gives a new graph G' , on the right-hand side of Figure 9. This is a form of star-triangle (or $Y - \Delta$) move.

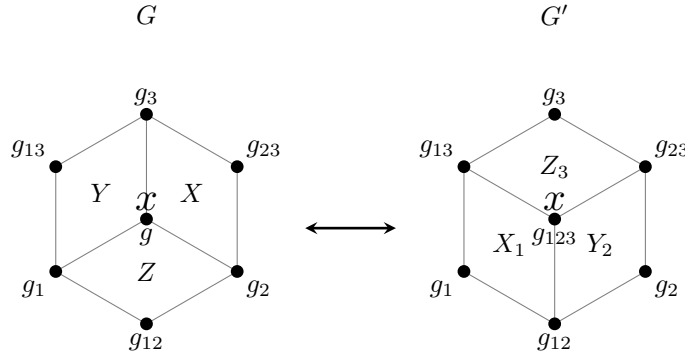


Figure 9: Cube flip at x .

When such a move is performed, we allow g_x to change into a new value g'_x ; let g' be the set of variables equal to g everywhere except at x where it is g'_x .

By labeling the g variables around x as in Figure 9, we say that g satisfies Kashaev's recurrence at x when g, g_1, \dots, g_{123} satisfy (2). Note that performing cube flips at x twice with g satisfying Kashaev's recurrence would bring back the original graph and constants, because of Proposition 2.

Theorem 2. *When g satisfies Kashaev's recurrence at x ,*

$$\frac{1}{g_x^2} \mathcal{Z}_{\text{m.loop}}^G(g) = \frac{1}{(g'_x)^2} \mathcal{Z}_{\text{m.loop}}^{G'}(g').$$

Another way to phrase this is to say that the Yang-Baxter equations for the $C_2^{(1)}$ loop model, as defined in [36], taken in our parametrization, become equivalent to Kashaev's recurrence.

Proof. There are six dual edges incoming in the region at x . We call *connection pattern* any way to color, label and connect these six incoming edges. For example, in the first row of Figure 10, the connection pattern is the following: all edges are all colored in blue; the west and northwest edges are labeled k and connected; the east and northeast edges are labeled l and connected; the southeast and southwest edges are labeled m and connected.

We want to construct a coupling between marked $C_2^{(1)}$ loops on G and on G' so that they agree everywhere except inside the changed region around x , and such that the connection pattern doesn't change. Thus we want to group the marked loop configurations on G and on G' according to their connection pattern. All possible cases are listed in Figure 10; indices on loops are arbitrary and we used the notation \hat{k} for the index different from k (so $\hat{A} = B$, $\hat{B} = A$, $\hat{0} = 2$, $\hat{2} = 0$). We omitted a few cases: first, the ones that can be derived from represented ones by a simple rotation, symmetry or color swap; secondly, for any row $i \in \{1, \dots, 7\}$, there is a dual row obtained by taking the right-hand side configurations of i , turning them upside-down and drawing them on the left - and similarly for the other side (notice that rows 2, 6, 7 are self-dual).

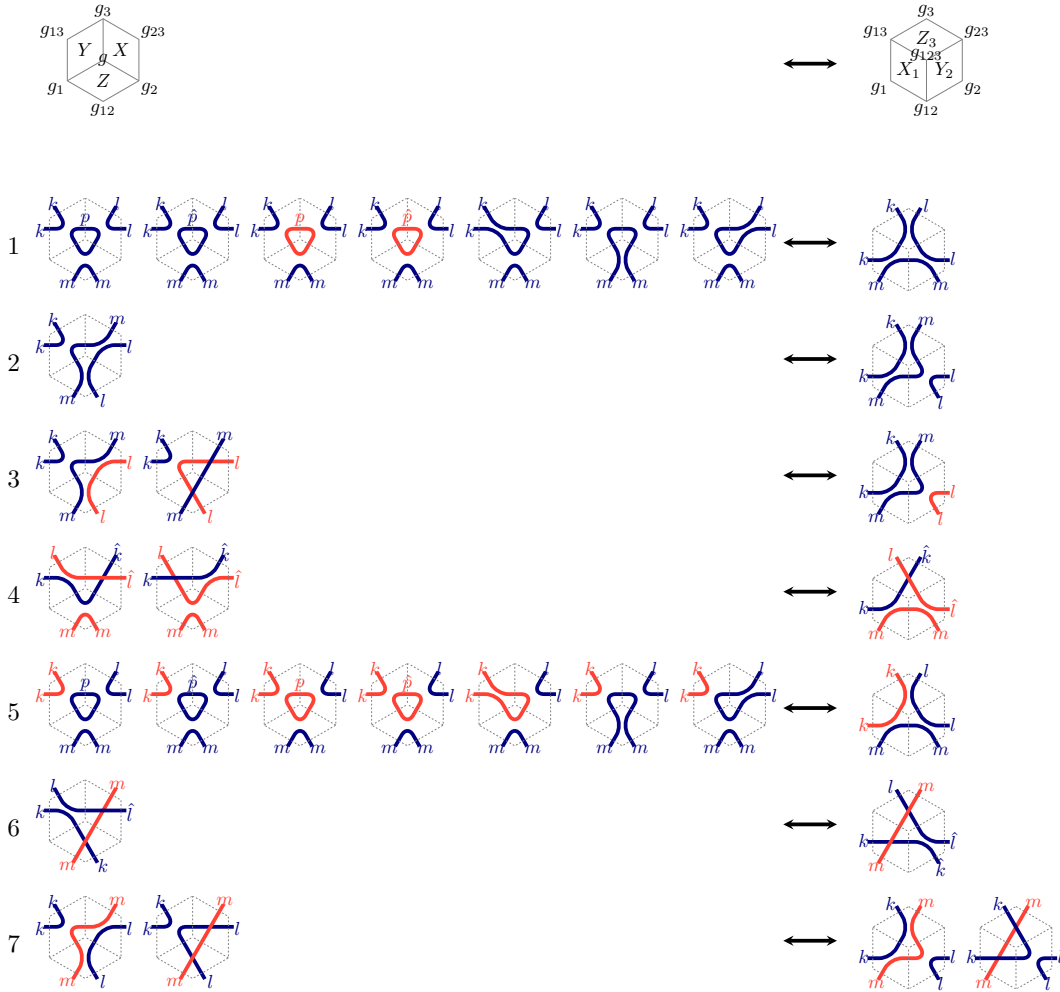


Figure 10: Correspondence between marked loops on G (left) and G' (right) having the same connection pattern.

Note that connection patterns are the same for G and G' . Let m be the total number of connection patterns, and let $\{1, \dots, m\}$ be a set of indices representing them. For any $j \in \{1, \dots, m\}$, let Σ_j be the set

of marked $C_2^{(1)}$ loop configurations on G having that connection pattern. Then $\Sigma_1, \dots, \Sigma_m$ are a partition of the set of all marked configurations on G . Thus in terms of partition functions we have

$$\mathcal{Z}_{\text{m.loop}}^G(g) = \sum_{j=1}^m \mathcal{Z}_j$$

where $\mathcal{Z}_j = \sum_{\sigma \in \Sigma_j} w_{\text{m.loop}}^G(\sigma)$. Similarly,

$$\mathcal{Z}_{\text{m.loop}}^{G'}(g) = \sum_{j=1}^m \mathcal{Z}'_j$$

where $\mathcal{Z}'_j = \sum_{\sigma \in \Sigma'_j} w_{\text{m.loop}}^{G'}(\sigma)$, and Σ'_j being the set of marked $C_2^{(1)}$ loop configurations on G' having connection pattern j .

If $\sigma \in \Sigma_j$, then its total weight can be written as

$$w_{\text{m.loop}}^G(\sigma) = a(\sigma)w_{\text{loc.}}(\sigma)$$

where $w_{\text{loc.}}(\sigma) = w_{i_1}^X w_{i_2}^Y w_{i_3}^Z$, with $(X, i_1), (Y, i_2), (Z, i_3) \in \sigma$; this is the local weight coming from the faces around x , and $a(\sigma)$ doesn't depend on the local configuration around x . Actually, if two local configurations have the same connection pattern, the possible ways to extend them to construct a loop configuration are the same, so the possible values of $a(\sigma)$ for these configurations are the same. This shows that \mathcal{Z}_j can be factored into:

$$\mathcal{Z}_j = A_j \left(\sum_{\sigma \in L_j} w_{\text{loc.}}(\sigma) \right), \quad (18)$$

where A_j is the sum of weight of all possible $a(\sigma)$ for any $\sigma \in \Sigma_j$, and L_j is the set of all local configurations around x in G that have connection pattern j .

Similarly, \mathcal{Z}'_j takes the form

$$\mathcal{Z}'_j = A_j \left(\sum_{\sigma \in L'_j} w_{\text{loc.}}(\sigma) \right). \quad (19)$$

Notice that the part A_j is the same for \mathcal{Z}_j and \mathcal{Z}'_j : indeed, G and G' are the same outside of the region around x ; given a local configuration in that region, the list of possible extensions into a global loop configuration only depends on its connection pattern.

As a result, the following lemma is sufficient to conclude the proof.

Lemma 3. *For any row $i \in \{1, \dots, 7\}$ in Figure 10, let L_i (resp. L'_i) be the list of local configurations in row i on G (resp. G'). If g satisfies Kashaev's recurrence, then*

$$\frac{1}{g_x^2} \sum_{\sigma \in L_i} w_{\text{loc.}}(\sigma) = \frac{1}{(g'_x)^2} \sum_{\sigma \in L'_i} w_{\text{loc.}}(\sigma).$$

Proof. For $i = 1$, L_1 contains 7 configurations, and the sum of their local weights is, in the same order as in Figure 10 (using the notations g, g_1, \dots, g_{123} like in Figure 9),

$$\begin{aligned} \frac{1}{g_x^2} \sum_{\sigma \in L_1} w_{\text{loc.}}(\sigma) &= \frac{2g_1^2 g_2^2 g_3^2}{g^2} + \frac{2g_1 g_2 g_3 X Y Z}{g^2} + \frac{g_1 g_2^2 g_3 g_{13}}{g} + \frac{g_1 g_2 g_3^2 g_{12}}{g} + \frac{g_1^2 g_2 g_3 g_{23}}{g} \\ &= g_1 g_2 g_3 \left(\frac{2g_1 g_2 g_3 + g(g_1 g_{23} + g_2 g_{13} + g_3 g_{12}) + 2XYZ}{g^2} \right). \end{aligned} \quad (20)$$

There is only one configuration in L'_1 which has local weight:

$$\frac{1}{(g'_x)^2} \sum_{\sigma \in L'_1} w_{\text{loc.}}(\sigma) = g_1 g_2 g_3 g_{123}. \quad (21)$$

The equality of (21) and (20) is given by Item 1 in Proposition 1.

The other cases are similar, using the various relations of Proposition 1. This is done in Appendix A. \square

Because of the self-duality property (Proposition 2) and the symmetries of the model, Lemma 3 is also true for any represented or non-represented row. Since connection patterns of configurations on G and G' are the same, the boundary conditions (if any) are preserved by this coupling. This concludes the proof of Theorem 2 \square

Remark 2. Based on Theorem 2, it is natural to define a renormalized partition function

$$\mathcal{Y}_{m.\text{loop}}^G(g) = \left(\prod_{x \in V} \frac{1}{g_x^2} \right) \mathcal{Z}_{m.\text{loop}}^G(g).$$

We can also go back to unmarked loops, weighted by a factor 2^{N_σ} (5), so that

$$\mathcal{Y}_{\text{loop}}^G(g) = \mathcal{Y}_{\text{loop}}^{G'}(g'). \quad (22)$$

This quantity will appear again as the combinatorial object representing the solution of Kashaev's recurrence on a stepped surface.

Remark 3. In the language of statistical physics, Theorem 2 is a case of Z -invariance. Since marked loops generalize unmarked loops as well as dimers, Z -invariance for marked loops under Kashaev's recurrence implies Z -invariance for unmarked loops, and (when the boundary conditions, if any, don't involve red connections) for the double dimer model of Theorem 1 for parametrized weights (17).

This particular dimer model is represented in Figure 11. After performing gauge transformations (by multiplying weights by $\frac{1}{\sqrt{g_x g_u}}$ around any vertex of G^Q that is closest to the edge $\{xu\}$ of G), we get the weights on the right of Figure 11. This is the dimer model of [29] in the particular case of Kashaev's relation; we get an alternative proof of its Z -invariance.

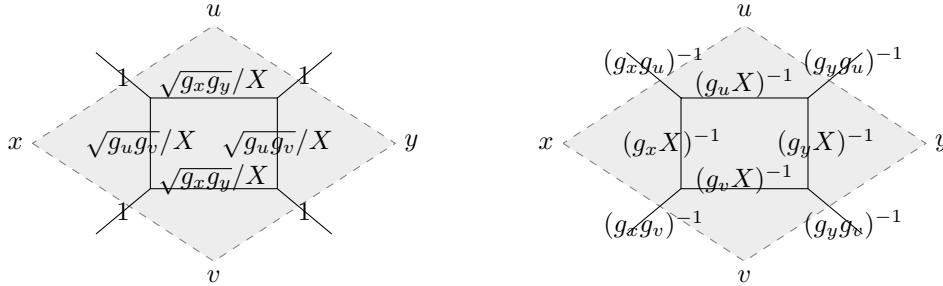


Figure 11: The dimer model's weights before (left) and after (right) gauge transformations. Here we have set $X = \sqrt{g_x g_y + g_u g_v}$.

Interestingly enough, if one starts from Kashaev's parametrized Ising model (1), and applies the procedure transforming Ising models into dimers on G^Q [13, 4], one gets the same dimer model as in Figure 11. However, the transformation between Ising model and dimers is not a direct mapping, so it is not completely clear in that setting why the Yang-Baxter equations for the Ising model translate into the same equations for dimers.

4 Taut configurations on stepped surfaces

We now turn to the study of *taut* configurations, which will be the appropriate objects counted by the solution of Kashaev's recurrence for arbitrary initial conditions.

4.1 Stepped surfaces

We denote by (e_1, e_2, e_3) the canonical basis of \mathbb{R}^3 . For $x = (i, j, k) \in \mathbb{Z}^3$, let $C_x \subset \mathbb{R}^3$ be the unit cube $[i, i + 1] \times [j, j + 1] \times [k, k + 1]$.

We call *stepped solid* a union of such unit cubes. A stepped solid U is said to be *monotone* if, for every $C_{(i,j,k)} \subset U$, and for every $i' \leq i, j' \leq j, k' \leq k$, $C_{(i',j',k')} \subset U$.

In this section, we always assume that U is a monotone stepped solid. In that case, the topological boundary ∂U is a union of squares of the form $(x, x + e_i, x + e_i + e_j, x + e_j)$ where $x \in \mathbb{Z}^3$ and $1 \leq i < j \leq 3$; it is called a *stepped surface*. This boundary naturally corresponds to an infinite planar quadrangulation $G(U)$, formally defined by the following sets of vertices and edges:

$$V(U) = \{x \in U \cap \mathbb{Z}^3 \mid x + e_1 + e_2 + e_3 \notin U\},$$

$$E(U) = \{\{x, y\} \mid x, y \in V, x - y \in \{\pm e_1, \pm e_2, \pm e_3\}\}.$$

We will also denote $F(U)$ the set of faces of $G(U)$.

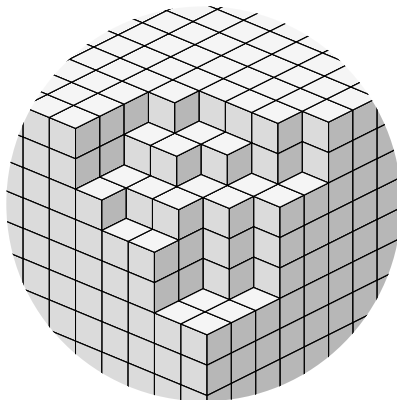


Figure 12: A portion of a stepped solid U .

4.2 Boundary conditions

To define a loop model on $G(U)$ we need some extra boundary conditions. Consider the negative corner $U_0 = \mathbb{R}_- \times \mathbb{R}_- \times \mathbb{R}_-$. We require that $U \subset U_0$ and that $U_0 \setminus U$ be composed of finitely many cubes. In this case, we say that U is *regular* (see Figure 12 for example). The infinite graph $G(U)$ is then equal to $G(U_0)$ outside of a sufficiently big ball for the euclidean distance centered at the origin. Let $B(O, R_U)$ be such a ball.

If U is a regular stepped solid, and $(g_x)_{x \in V(U)}$ is a collection of variables on the vertices of $G(U)$, then Kashaev's recurrence (2) is enough to recursively define g on $\mathbb{Z}^3 \setminus U$. Then, the value at the origin $g_{(0,0,0)}$ is called the *solution of Kashaev's recurrence* with initial conditions $(g_x)_{x \in V(U)}$.

On $G(U_0)$ let σ_0 be the configuration given in Figure 13. Following the terminology of [29], we say that a $C_2^{(1)}$ loop configuration σ on $G(U)$ is *taut* when it has the same connectivity as σ_0 on a neighborhood of

infinity – meaning that outside of a ball of radius $R_\sigma \geq R_U$, σ has to be equal to σ_0 , and σ has to contain paths connecting the edges of $U \cap B(O, R_\sigma)$ that are connected in σ_0 . This is the case in Figure 3 for example.

Let $\Sigma(U)$ be the set of taut $C_2^{(1)}$ loop configuration on $G(U)$.

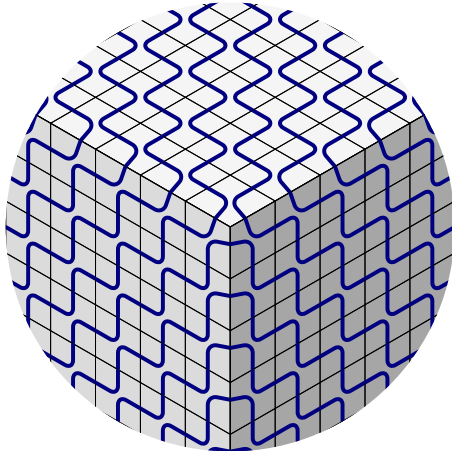


Figure 13: The initial stepped solid U_0 and initial configuration σ_0 .

The following lemmas are direct adaptations of Carroll and Speyer’s arguments on cube groves [5].

Lemma 4. $\Sigma(U_0)$ only contains σ_0 .

Proof. Let σ be a taut configuration on $G(U_0)$. Suppose that it is different from σ_0 . Without loss of generality, we can assume that there is a face f of the form $\{x, x + e_1, x + e_1 + e_2, x + e_2\}$ that differs from σ_0 . Take such a face with $x = (i, j, 0)$ and $i + j$ minimal; this is possible because σ is equal to σ_0 for all faces far enough from the origin. Then the faces $f - e_1$ and $f - e_2$ have to be the same for σ and σ_0 , which implies that the dual edges of $\{x, x + e_1\}$ and $\{x, x + e_2\}$ are blue. Now since σ differs from σ_0 on f , the only possible local configurations connect these two blue edges inside of f . This implies that the connectivity of σ differs from the one in σ_0 , which contradicts the definition of a taut configuration. \square

Note that a configuration σ contains two types of paths: infinite simple paths, and finite closed simple loops. In the rest of the paper, the latter will simply be called “loops”.

Lemma 5. For a regular stepped solid U , $\Sigma(U)$ is finite. Moreover, a taut $C_2^{(1)}$ loop configuration on U has a finite number of loops.

Proof. Let $\sigma \in \Sigma(U)$. We know that σ has the same connectivity as σ_0 and is equal to σ_0 outside of $B(O, R_\sigma)$. By the same argument described in the proof of Lemma 4, σ actually has to be equal to σ_0 outside of $B(O, R_U)$. For a fixed U , there is only a finite number of such σ , and their loops have to be in $B(O, R_U)$ so there is a finite number of them. \square

4.3 Weights

Let U be a regular stepped solid, and let $(g_x)_{x \in V(U)}$ be a collection of variables on the vertices of $G(U)$ that can be thought of as positive real numbers. For a taut $C_2^{(1)}$ loop configuration $\sigma \in \Sigma(U)$, we still denote N_σ its number of loops. Let us consider the weight:

$$w_{\text{taut}}^U(\sigma) = 2^{N_\sigma} \left(\prod_{(f, i_k) \in \sigma} w_i^f \right) \left(\prod_{x \in V(U)} \frac{1}{g_x^2} \right), \quad (23)$$

where the local weights w_i^f are defined using parametrization (17). This expression makes sense because N_σ is finite (Lemma 5) and $\prod w_i^f$ formally makes g_x appear with exponent 2 for every x in the “flat” region where $\sigma = \sigma_0$, so the two products cancel out for all but a finite number of terms. For example, $w_{\text{taut}}^{U_0}(\sigma_0) = g_{(0,0,0)}$.

Since the number of taut configurations is finite (Lemma 5), we can define the renormalized partition function:

$$\mathcal{Y}_{\text{taut}}^U(g) = \sum_{\sigma \in \Sigma(U)} w_{\text{taut}}^U(\sigma).$$

Formally, $\mathcal{Y}_{\text{taut}}^U(g)$ is simply a Laurent polynomial in the g variables and in the $\sqrt{g_x g_y + g_u g_v}$ variables, for any face bordered by x, u, y, v ; we call these *face variables*.

Theorem 3. *Let U be a regular stepped solid, and $(g_x)_{x \in V(U)}$ be a collection of variables on the vertices of $G(U)$. Then the solution of Kashaev’s recurrence at the origin with initial condition $(g_x)_{x \in V(U)}$ is*

$$g_{(0,0,0)} = \mathcal{Y}_{\text{taut}}^U(g).$$

Proof. Let g be the solution of Kashaev’s recurrence with initial conditions on $V(U)$ (so that g is also defined on $\mathbb{Z}_-^3 \setminus U$).

The results of Section 3 imply that the renormalized partition function $\mathcal{Y}_{\text{taut}}^U(g)$ doesn’t change when a cube is added to, or removed from, U in such a way that it remains a stepped solid - as long as we keep using the g variables. Indeed, the boundary conditions are unchanged when a cube flip is performed so all the computations stay the same for taut configurations.

By repeatedly removing cubes starting from U_0 to get to U , this implies

$$\mathcal{Y}_{\text{taut}}^U(g) = \mathcal{Y}_{\text{taut}}^{U_0}(g).$$

But $\Sigma(U_0)$ only contains σ_0 (Lemma 4), and $w_{\text{taut}}^{U_0}(\sigma_0) = g_{(0,0,0)}$, so that $\mathcal{Y}_{\text{taut}}^{U_0}(g) = g_{(0,0,0)}$. \square

4.4 Algebraic consequences

We have seen that the solution of Kashaev’s recurrence is equal to the partition function $\mathcal{Y}_{\text{taut}}^U(g)$. However, several taut $C_2^{(1)}$ loop configurations on $G(U)$ might correspond to the same monomial in $\mathcal{Y}_{\text{taut}}^U(g)$. The following Theorem states that it is not the case, and gives consequences on the exponents and coefficients appearing in the Laurent polynomial. The first and third points were already obtained in [29] (Theorem 7.8) by an indirect method.

Theorem 4. *For any formal initial condition $(g_x)_{x \in V(U)}$ where U is a regular stepped solid, let $g_{(0,0,0)}$ be the solution at the origin of Kashaev’s recurrence. Then:*

1. $g_{(0,0,0)}$ is a Laurent polynomial in the $(g_x)_{x \in V(U)}$ vertex variables and in the face variables defined on the faces of $G(U)$;
2. The monomials are in one-to-one correspondence with taut $C_2^{(1)}$ loop configurations on U ;
3. The g variables appear with exponent in $\{-2, \dots, 4\}$. The face variables appear with exponent in $\{0, 1\}$;
4. The coefficients in front of monomials are powers of 2.

Proof. For any $\sigma \in \Sigma(U)$ and $x \in V(U)$, the g_x variable appears with an integer exponent in $w_U(\sigma)$. Indeed, it gets an exponent $\frac{1}{2}$ when, and only when, the color of the loops change around x (see the weights (17) and (23)), and this happens an even number of times. The first point is thus a direct consequence of Theorem 3.

The third point comes from the observation that any vertex belongs to at most 6 faces of $G(U)$, so its exponent is between $0 - 2$ and $6 - 2$. The face variables can only appear once and with exponent 1.

The last point is a direct consequence of the second point, so all that remains to be proved is the following statement:

Let $\sigma, \sigma' \in \Sigma(U)$ be two taut $C_2^{(1)}$ loop configurations on $G(U)$. If the following expressions in the formal g variables are equal:

$$\left(\prod_{(f,i_k) \in \sigma} w_i^f \right) \left(\prod_{x \in V(U)} \frac{1}{g_x^2} \right) = \left(\prod_{(f,i_k) \in \sigma'} w_i^f \right) \left(\prod_{x \in V(U)} \frac{1}{g_x^2} \right) \quad (24)$$

then $\sigma = \sigma'$.

To prove this, we give a procedure to reconstruct σ from the monomial in the left-hand side of (24).

Suppose that there is a vertex $x \in \mathbb{Z}^3$ so that σ is already known on every face around x except for one, which we call f . We claim that we can find $\sigma|_f$. To do so, first we look whether the face variable associated to f is present in the monomial. If it is present, then the local configuration of σ at f belongs to the third or fourth row of (17); otherwise it belongs to the first, second or fifth row. Then we look at the exponent of g_x that doesn't come from already known faces: in the first case it can be $\frac{1}{2}$ (third row) or 0 (fourth row). In the second case it can be 1 (first row), 0 (second row) or $\frac{1}{2}$ (fifth row), so now we know which row $\sigma|_f$ belongs to. There are two local configurations in this row. To know which one it is, just look at the color of an incoming edge that is already known.

Since σ is taut, we already know it outside of a sufficiently big ball centered at the origin. We want to use the previous argument to successively discover new faces, until σ is known everywhere. To do so, we need to show that there is always an x that satisfies the first statement of the previous paragraph. Any x having degree 2 on the boundary of the graph formed by currently unknown faces would do the trick.

We prove that such an x always exists by showing a slightly more general result on *lozenge graphs*. A lozenge graph is a finite planar quadrangulation such that all internal faces are non-degenerate rhombi with same edge length. We call *outer boundary* of a lozenge graph the set of edges separating a face from the infinite connected component of the complement of the graph in the plane.

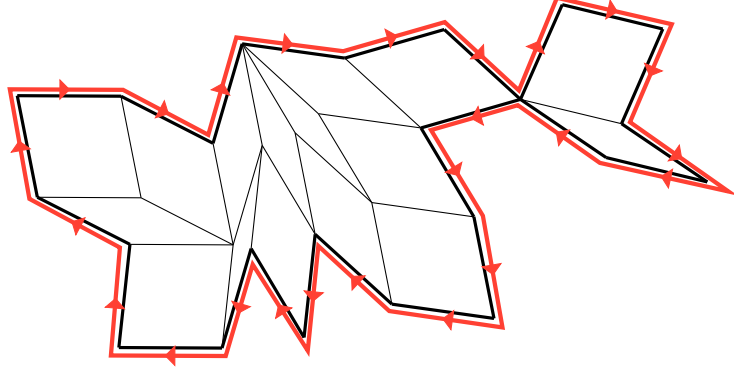


Figure 14: A connected lozenge graph and its oriented outer boundary.

Lemma 6. *Any non-empty lozenge graph has at least three vertices of degree 2 on its outer boundary.*

Proof. Let G be a lozenge graph. By restricting ourselves to a connected component, we can assume that G is connected. Let x_1 be a vertex on the boundary of G . We orient the boundary clockwise, meaning that we orient each of its edges so that the infinite connected component is on the left, see Figure 14. Starting from x_1 , we follow the boundary by taking the leftmost edge when several outgoing edges are present. We denote (x_1, \dots, x_p, x_1) this closed path, which is a single oriented curve around G , with possible pinches (some of the x_i vertices may be equal). We also take $x_0 := x_p$.

For any $i \in \{1, \dots, p\}$, the edge $\{x_{i-1}, x_i\}$ belongs to exactly one rhombus (otherwise it would not be on the boundary). Let u_i be the vertex of that lozenge that is diagonally opposite to x_{i-1} . Similarly, let v_i be the vertex that is diagonally opposite to x_{i+1} in the rhombus that contains the edge $\{x_i, x_{i+1}\}$; see Figure 15.

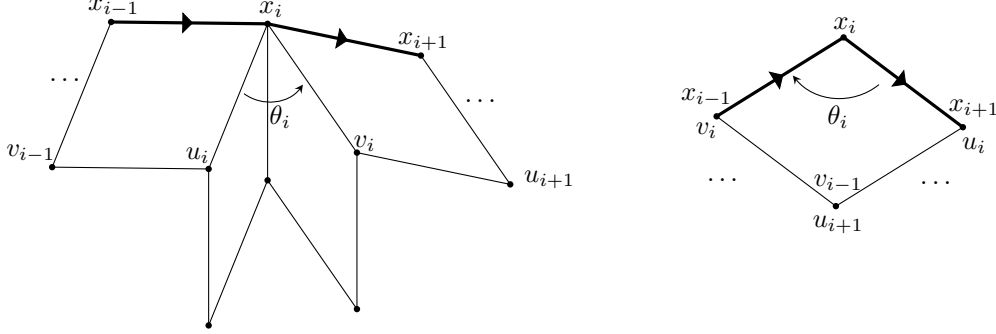


Figure 15: The u_i, v_i vertices and θ_i angle when x_i has degree > 2 (left) or 2 (right).

Let θ_i be

$$\theta_i = \angle(\overrightarrow{x_i x_{i-1}}, \overrightarrow{x_i x_{i+1}}) - \angle(\overrightarrow{x_i x_{i-1}}, \overrightarrow{x_i u_i}) - \angle(\overrightarrow{x_i v_i}, \overrightarrow{x_i x_{i+1}}),$$

where the three angles are taken in $]0, 2\pi[$. Clearly, θ_i is equal to $\angle(\overrightarrow{x_i u_i}, \overrightarrow{x_i v_i})$ modulo 2π . By checking all possible cases like in Figure 15, we can be more precise:

- when x_i does not have degree 2 in G , $\theta_i \in]0, 2\pi[$,
- otherwise, $\theta_i \in]-\pi, 0[$.

Our goal is to show that the sum of these angles is -2π , so that at least three of them have to be negative, and we can conclude.

Notice that $\overrightarrow{x_i v_i} = \overrightarrow{x_{i+1} u_{i+1}}$. By using this fact and reorganizing the sums we get:

$$\begin{aligned} \sum_{i=1}^p \theta_i &= \sum_{i=1}^p \angle(\overrightarrow{x_i x_{i-1}}, \overrightarrow{x_i x_{i+1}}) - \sum_{i=1}^p \angle(\overrightarrow{x_i x_{i-1}}, \overrightarrow{x_i u_i}) - \sum_{i=1}^p \angle(\overrightarrow{x_{i+1} u_{i+1}}, \overrightarrow{x_i x_{i+1}}) \\ &= \sum_{i=1}^p \angle(\overrightarrow{x_i x_{i-1}}, \overrightarrow{x_i x_{i+1}}) - \sum_{i=1}^p (\angle(\overrightarrow{x_i x_{i-1}}, \overrightarrow{x_i u_i}) + \angle(\overrightarrow{x_i u_i}, \overrightarrow{x_{i-1} x_i})). \end{aligned}$$

By the choice of angles, $\angle(\overrightarrow{x_i x_{i-1}}, \overrightarrow{x_i u_i}) + \angle(\overrightarrow{x_i u_i}, \overrightarrow{x_{i-1} x_i})$ is equal to π , so we have:

$$\sum_{i=1}^p \theta_i = \sum_{i=1}^p (\angle(\overrightarrow{x_i x_{i-1}}, \overrightarrow{x_i x_{i+1}}) - \pi).$$

Now the angles $\angle(\overrightarrow{x_i x_{i-1}}, \overrightarrow{x_i x_{i+1}}) - \pi$ are the oriented angles $\angle(\overrightarrow{x_{i-1} x_i}, \overrightarrow{x_i x_{i+1}})$ taken in $] -\pi, \pi[$. Since the boundary (x_1, \dots, x_p, x_1) is a clockwise oriented closed curve, they sum up to -2π , so that

$$\sum_{i=1}^p \theta_i = -2\pi$$

as claimed. □

This concludes the proof of Theorem 4. □

4.5 Limit shapes

The existence of limit shapes is shown exactly as in [29]. We just do the computations here to show how it fits into our particular framework. See also [33, 11, 19] for similar proofs in the case of the octahedron and cube recurrences.

For $v = (i, j, k) \in \mathbb{Z}^3$, we define its *height* as $h(v) = i + j + k$.

For $N \in \mathbb{Z}^+$, let U_N be the following regular stepped solid:

$$U_N = \{C_v \mid v \in (\mathbb{Z}^-)^3, h(v) \leq -N\}.$$

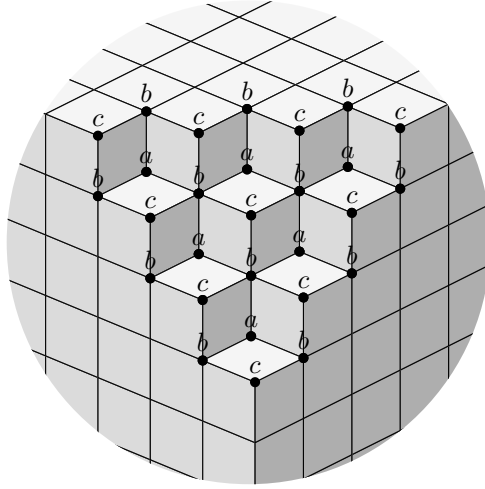


Figure 16: The stepped solid U_3 and periodic weights on the vertices.

We put a periodic g function on the vertices $V(U_N)$ that only depends on the height of vertices (see Figure 16). The values of g in the flat regions don't appear in the weight of a taut configuration so they may be chosen arbitrarily. Our aim is to describe the shape of a random taut loop configuration on $G(U_N)$ sampled proportionally to its weight, when N is large.

Instead of letting N change, it will be convenient to consider instead the infinite stepped solid

$$U = \{C_v \mid h(v) \leq 2\},$$

represented in Figure 17, and to see it from some $x \in \mathbb{Z}^3$ of positive height, and to let x change. Thus for any $x \in \mathbb{Z}^3$, we consider the “regular” stepped solid

$$U_x = U \cap (x + U_0).$$

Up to a translation of vector $-x$, U_x is a regular stepped solid, similar to U_N where $N = h(x) - 2$ for $h(x) \geq 3$.

Let $g^{a,b,c}$ denote the set of initial conditions of Figure 17:

$$g^{a,b,c}(x) = \begin{cases} a & \text{if } h(x) = 0, \\ b & \text{if } h(x) = 1, \\ c & \text{if } h(x) = 2. \end{cases}$$

Using these weights, we can define a partition function of loops on U_x :

$$Y_x = \mathcal{Y}_{\text{taut}}^{U_x}(g^{a,b,c}).$$

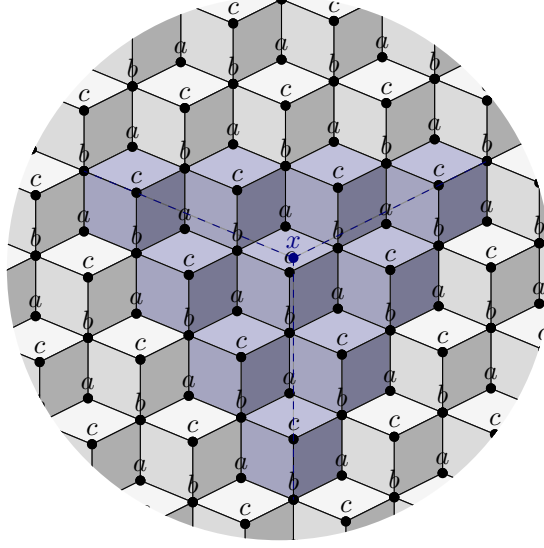


Figure 17: The infinite stepped solid U with vertex weights $g^{a,b,c}$, an x of height 5 and the associated U_x (in blue). The origin $(0, 0, 0)$ is one of the a variables.

Of course Y_x depends only on the height of x . If $h(x) = N$, we simply denote $Y_N = Y_x$. We also define $X_N = \sqrt{Y_N Y_{N+2} + Y_{N+1}^2}$. These quantity can be exactly computed using Kashaev's relation for a function depending only on height, see [29], Section 7.5. The result is the following.

Let $R = \frac{ac}{b^2}$ and $S = \frac{bd}{c^2}$, where $d = \frac{2b^3 + 3abc + 2(ac+b^2)^{\frac{3}{2}}}{a^2}$. As a side note, S and R can be deduced from one another as the greatest root of the intrinsic relation

$$R^2 S^2 - 6RS - 4R - 4S - 3 = 0.$$

We have:

$$\begin{aligned} Y_{2n} &= a^{1-2n} b^{2n} R^{n^2} S^{n^2-n}, \\ Y_{2n+1} &= a^{-2n} b^{2n+1} R^{n^2+n} S^{n^2}, \\ X_{2n} &= \sqrt{1+R} Y_{2n+1}, \\ X_{2n+1} &= \sqrt{1+S} Y_{2n+2}. \end{aligned}$$

We are interested in the quantity

$$\rho(x) = \left(g_{(0,0,0)} \frac{\partial \log \left(\mathcal{Y}_{\text{taut}}^{U_x}(g) \right)}{\partial g_{(0,0,0)}} \right) \Big|_{g=g^{a,b,c}}. \quad (25)$$

This quantity has a probabilistic meaning. If σ is a random taut loop configuration on $G(U_x)$ chosen proportionally to its weight $w_{\text{taut}}^{U_x}(\sigma)$ for the initial conditions $g^{a,b,c}$, let n_0 be the power of $g_{(0,0,0)}$ appearing in the formal weight of σ . For a face f , let $\epsilon_f(\sigma)$ be 1 if $\sigma|_f$ is in the third or fourth row in Figure 2, and 0 otherwise. Then

$$\rho(x) = \mathbb{E} \left[n_0 + \frac{1}{2(1+R)} \sum_{f \in F \text{ around } (0,0,0)} \epsilon_f(\sigma) \right]. \quad (26)$$

If we looked instead at U_N for $N = h(x) - 2$, by a simple symmetry, this quantity would be equal to the same expectation on the vertex $-x$ instead of 0 (and this vertex would have to be of type a in U_N). By

defining the same partial derivative as in (25) with respect to $g_{(1,0,0)}$ or $g_{(1,1,0)}$, we could keep track of similar observables for vertices of type b and c . We will not make use of the exact formula of that observable, we just use it to show that the behavior of loops changes depending on the vertex of U_N .

The observable ρ is defined as some logarithmic derivative of the partition function $\mathcal{Y}_{\text{taut}}^{U_x}$. By taking the logarithmic derivative of Kashaev's relation (15), which is satisfied by $\mathcal{Y}_{\text{taut}}^{U_x}$, and evaluating at the initial condition $g^{a,b,c}$, we get linear relations on ρ :

$$\begin{aligned} \text{if } h(x) \text{ is even, } \rho(x + e_1 + e_2 + e_3) = & \alpha\rho(x) + \beta(\rho(x + e_1) + \rho(x + e_2) + \rho(x + e_3)) \\ & + \gamma(\rho(x + e_1 + e_2) + \rho(x + e_1 + e_3) + \rho(x + e_2 + e_3)), \end{aligned} \quad (27)$$

$$\begin{aligned} \text{if } h(x) \text{ is odd, } \rho(x + e_1 + e_2 + e_3) = & \alpha'\rho(x) + \beta'(\rho(x + e_1) + \rho(x + e_2) + \rho(x + e_3)) \\ & + \gamma'(\rho(x + e_1 + e_2) + \rho(x + e_1 + e_3) + \rho(x + e_2 + e_3)), \end{aligned} \quad (28)$$

where

$$\begin{aligned} \alpha &= \frac{3 + 3\sqrt{1+R} - 2RS}{RS}, & \beta &= \frac{2 + 2\sqrt{1+R} + R}{R^2S}, & \gamma &= \frac{1 + \sqrt{1+R}}{RS}, \\ \alpha' &= \frac{3 + 3\sqrt{1+S} - 2RS}{RS}, & \beta' &= \frac{2 + 2\sqrt{1+S} + R}{RS^2}, & \gamma' &= \frac{1 + \sqrt{1+S}}{RS}. \end{aligned}$$

Let us define the generating function:

$$F(x, y, z) = \sum_{(i,j,k) \in \mathbb{Z}^3, h(i,j,k) \geq 0} \rho(i, j, k) x^i y^j z^k.$$

Using (27) (28), it is straightforward to compute F . It is a rational function of the form

$$F(x, y, z) = \frac{P(x, y, z)}{H(x, y, z)}$$

where P is some polynomial and

$$\begin{aligned} H(x, y, z) = & (\alpha xyz + \gamma(x + y + z)) (\alpha' xyz + \gamma'(x + y + z)) \\ & - (1 - \beta(xy + xz + yz)) (1 - \beta'(xy + yz + xz)). \end{aligned}$$

The coefficients $\alpha, \beta, \gamma, \alpha', \beta', \gamma'$ can all be defined using R so they are all dependent. Actually, by defining $\theta = \gamma\gamma'$, H takes the form:

$$H(x, y, z) = \theta(x^2 - 1)(y^2 - 1)(z^2 - 1) + (1 - \theta)(xy - 1)(xz - 1)(yz - 1).$$

At that point, we have recovered the denominator studied in [29]. The asymptotic behavior of the observables $\rho(i, j, k)$ can be obtained from the analysis of their generating function F at the singularity $(1, 1, 1)$ (Theorem 5.7 of [29], which is a corollary of various results of [32, 2]). Around that point, the leading homogeneous part of $H(1 + X, 1 + Y, 1 + Z)$ is

$$\bar{H}(X, Y, Z) = 2(1 + 3\theta)XYZ + (1 - \theta)(X^2Y + XY^2 + X^2Z + XZ^2 + Y^2Z + YZ^2).$$

Thus the limit shape of the model can be computed as the dual of the curve

$$X^2Y + XY^2 + X^2Z + XZ^2 + Y^2Z + YZ^2 + \lambda XYZ$$

where $\lambda = \frac{2(1+3\theta)}{1-\theta}$. See [29] for the computation of this dual, its shape, and the behavior of ρ depending on its position relatively to the limit shape. The dual is a projective curve in $P\mathbb{R}^3$, in the following figures we represent it in \mathbb{R}^3 intersected with the plane $x + y + z = -1$.

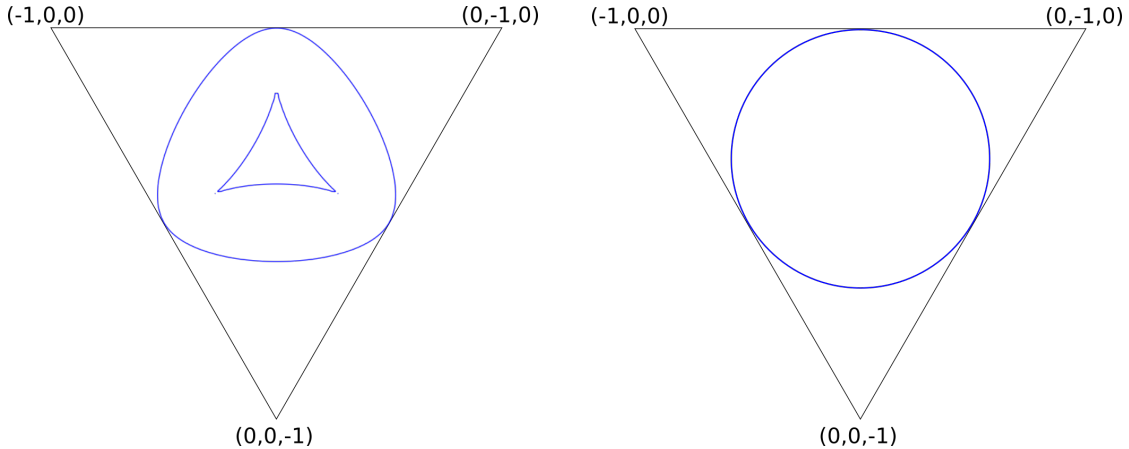


Figure 18: Limit shapes for $R = 0.2$ (left) and $R = 3$ (right).

We note that the limit shape only depends on R , and there is an extra symmetry: when R and S are exchanged, λ remains the same so the limit shape is the same. In general, $\lambda \in (2, 3]$. When $\lambda \neq 3$, the limit shape looks like a rounded triangle tangent to the borders of the carved section of U_N , with an internal facet; see Figure 18. The point $\lambda = 3$ is somehow critical and corresponds to $R = S = 3$. At that point, the limit shape becomes a circle and the central facet is reduced to a point.

We computed simulations of the model for different values of R in Figure 19. In the three corner regions ρ decays to 0 exponentially fast in N , which corresponds to the “frozen phase” where only infinite blue paths appear in the densest possible packing; it is possible to convince oneself that this is indeed the behavior implied by (26) being close to 0. The annular region around the facet corresponds to a “liquid phase” where ρ tends to 0 polynomially fast. It seems that this region’s interface with the central facet is delimited by the infinite blue paths closest to the center. In the central facet there is a “gaseous phase” where ρ tends to $\frac{1}{3}$, and the boundary conditions don’t appear any more.

4.6 Cube groves

Cube groves were introduced by Carroll and Speyer in [5]. They are essential spanning forests, often represented with their dual forest, on the graph consisting of the even vertices of $G(U)$ with edges on diagonals of the faces of the cubes. One example is displayed in black lines in Figure 21.

Let $\Sigma_0(U)$ be the subset of $\Sigma(U)$ containing all taut $C_2^{(1)}$ loop configurations $\sigma \in \Sigma(U)$ such that $N_\sigma = 0$, *i.e.* σ has no finite loop. Such a configuration cannot contain any red edge, since all red paths are finite loops. Thus σ can be represented by a subset of the diagonals of the faces of the cubes, as in Figure 20.

It is easy to check that this set of diagonals is necessarily a cube grove, and conversely, any cube grove corresponds to such a loop configuration (which is in fact the classical interface between the spanning forest and its dual). The transformation is thus a bijection between $\Sigma_0(U)$ and cubes groves on U . Moreover, this bijection is weight-preserving, in the sense that the weight of $\sigma \in \Sigma_0(U)$ is equal to the weight of its associated cube grove as defined by Carroll and Speyer, when their face variables are set to be equal to 1.

As a result, the partition function truncated to $\Sigma_0(U)$,

$$\mathcal{Y}_0^U \text{taut}(g) = \sum_{\sigma \in \Sigma_0(U)} w_{\text{taut}}^U(\sigma),$$

is formally equal to the solution of the cube recurrence with initial conditions on U . This is not such a surprise: on a field of characteristic 2, Kashaev’s relation (15) reduces to

$$gg_{123} + g_1g_{23} + g_2g_{13} + g_3g_{12} = 0,$$

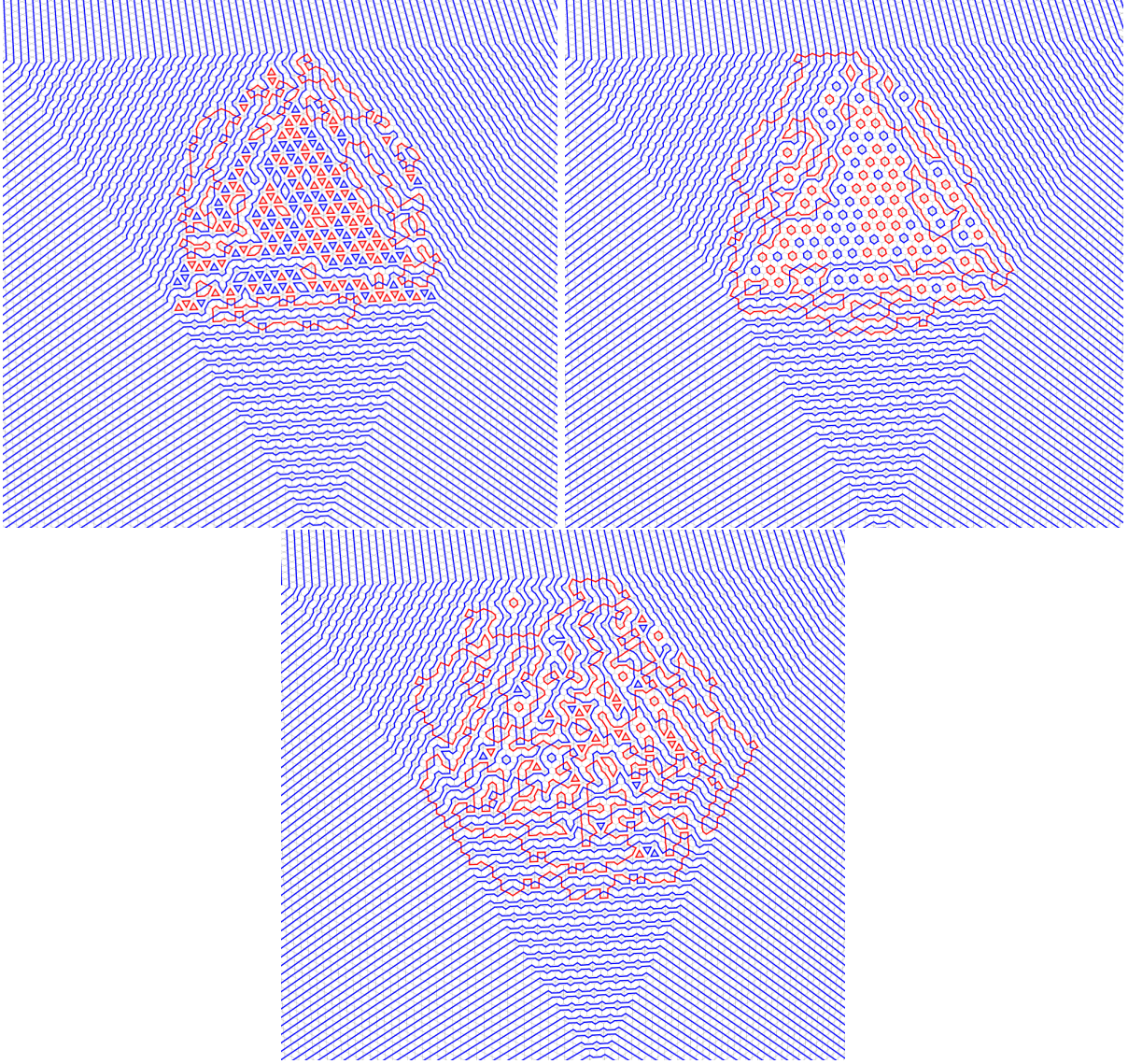


Figure 19: Simulations for $N = 40$, and $R = 0.2$ (top left), $R \simeq 130.7$ ($S = 0.2$) (top right), $R = 3$ (bottom). The first two simulations correspond to the same limit shape.

which is exactly the cube recurrence in characteristic 2, while $\mathcal{Y}_{\text{taut}}^U(g)$ reduces to $\mathcal{Y}_0^U(g)$.

A Calculations for Lemma 3

- $i = 2$:

$$\frac{1}{g_x^2} \sum_{\sigma \in L_2} w_{\text{loc}}(\sigma) = g_1 g_3 g_{12} g_{23},$$

$$\frac{1}{(g'_x)^2} \sum_{\sigma \in L'_2} w_{\text{loc}}(\sigma) = g_1 g_3 g_{12} g_{23}.$$

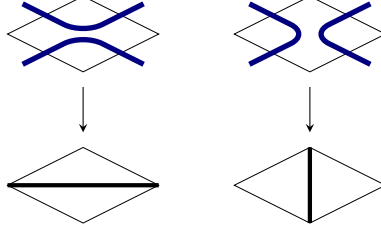


Figure 20: Local transformation from $\Sigma_0(U)$ to cube groves

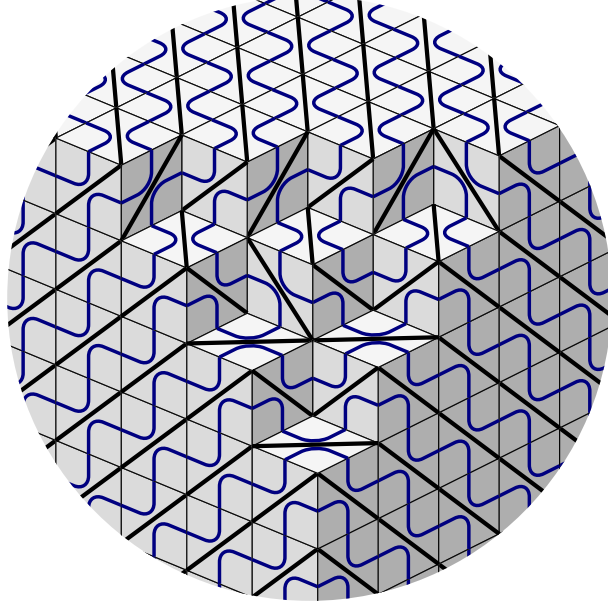


Figure 21: A configuration $\sigma \in \Sigma_0(U)$ and the corresponding cube grove.

- $i = 3$:

$$\begin{aligned} \frac{1}{g_x^2} \sum_{\sigma \in L_3} w_{\text{loc}}(\sigma) &= g^{-1} g_1 g_3 g_{12}^{\frac{1}{2}} g_{23}^{\frac{1}{2}} XZ + g^{-1} g_1 g_2 g_3 g_{12}^{\frac{1}{2}} g_{23}^{\frac{1}{2}} Y \\ &= g_1 g_3 g_{12}^{\frac{1}{2}} g_{23}^{\frac{1}{2}} \left(\frac{XZ + g_2 Y}{g} \right), \\ \frac{1}{(g'_x)^2} \sum_{\sigma \in L'_3} w_{\text{loc}}(\sigma) &= g_1 g_3 g_{12}^{\frac{1}{2}} g_{23}^{\frac{1}{2}} Y_2. \end{aligned}$$

The equality of $\frac{1}{(g'_x)^2} \sum_{\sigma \in L'_2} w_{\text{loc}}(\sigma)$ and $\frac{1}{g_x^2} \sum_{\sigma \in L_2} w_{\text{loc}}(\sigma)$ is equivalent to Item 3 of Proposition 1.

- $i = 4$:

$$\begin{aligned}\frac{1}{g_x^2} \sum_{\sigma \in L_4} w_{\text{loc}}(\sigma) &= g^{-1} g_1^{\frac{1}{2}} g_2 g_3^{\frac{1}{2}} g_{13}^{\frac{1}{2}} g_{23}^{\frac{1}{2}} YZ + g^{-1} g_1^{\frac{3}{2}} g_2 g_3^{\frac{1}{2}} g_{13}^{\frac{1}{2}} g_{23}^{\frac{1}{2}} X \\ &= g_1^{\frac{1}{2}} g_2 g_3^{\frac{1}{2}} g_{13}^{\frac{1}{2}} g_{23}^{\frac{1}{2}} \left(\frac{YZ + g_1 X}{g} \right), \\ \frac{1}{(g'_x)^2} \sum_{\sigma \in L'_4} w_{\text{loc}}(\sigma) &= g_1^{\frac{1}{2}} g_2 g_3^{\frac{1}{2}} g_{13}^{\frac{1}{2}} g_{23}^{\frac{1}{2}} X_1.\end{aligned}$$

The equality is equivalent to Item 2 of Proposition 1.

- $i = 5$:

$$\begin{aligned}\frac{1}{g_x^2} \sum_{\sigma \in L_5} w_{\text{loc}}(\sigma) &= 2g^{-2} g_1^{\frac{3}{2}} g_2^2 g_3^{\frac{3}{2}} Y + 2g^{-2} g_1^{\frac{3}{2}} g_2 g_3^{\frac{3}{2}} XZ + g^{-1} g_1^{\frac{1}{2}} g_2 g_3^{\frac{1}{2}} g_{13} XZ \\ &\quad + g^{-1} g_1^{\frac{3}{2}} g_2 g_3^{\frac{1}{2}} g_{23} Y + g^{-1} g_1^{\frac{1}{2}} g_2 g_3^{\frac{3}{2}} g_{12} Y \\ &= g_1^{\frac{1}{2}} g_2 g_3^{\frac{1}{2}} \left(\frac{2g_1 g_2 g_3 Y}{g^2} + \frac{2g_1 g_3 XZ}{g^2} + \frac{g_{13} XZ}{g} + \frac{g_1 g_{23} Y}{g} + \frac{g_3 g_{12} Y}{g} \right), \\ \frac{1}{(g'_x)^2} \sum_{\sigma \in L'_5} w_{\text{loc}}(\sigma) &= g_1^{\frac{1}{2}} g_2 g_3^{\frac{1}{2}} X_1 Z_3.\end{aligned}$$

Using Items 2 and 4 of Proposition 1, we get

$$\begin{aligned}X_1 Z_3 &= \left(\frac{g_1 X + YZ}{g} \right) \left(\frac{g_3 Z + XY}{g} \right) \\ &= \frac{g_1 g_3 XZ + g_1 X^2 Y + g_3 Y Z^2 + XY^2 Z}{g^2} \\ &= \frac{g_1 g_3 XZ + g_1 (g g_{23} + g_2 g_3) Y + g_3 (g g_{12} + g_1 g_2) Y + (g g_{13} + g_1 g_3) XZ}{g^2} \\ &= \frac{2g_1 g_2 g_3 Y}{g^2} + \frac{2g_1 g_3 XZ}{g^2} + \frac{g_{13} XZ}{g} + \frac{g_1 g_{23} Y}{g} + \frac{g_3 g_{12} Y}{g}\end{aligned}$$

and the equality follows.

- $i = 6$:

$$\begin{aligned}\frac{1}{g_x^2} \sum_{\sigma \in L_6} w_{\text{loc}}(\sigma) &= g_1^{\frac{1}{2}} g_2 g_3^{\frac{1}{2}} g_{12}^{\frac{1}{2}} g_{13}^{\frac{1}{2}} g_{23}^{\frac{1}{2}}, \\ \frac{1}{(g'_x)^2} \sum_{\sigma \in L'_6} w_{\text{loc}}(\sigma) &= g_1^{\frac{1}{2}} g_2 g_3^{\frac{1}{2}} g_{12}^{\frac{1}{2}} g_{13}^{\frac{1}{2}} g_{23}^{\frac{1}{2}}.\end{aligned}$$

- $i = 7$:

$$\begin{aligned}\frac{1}{g_x^2} \sum_{\sigma \in L_7} w_{\text{loc}}(\sigma) &= g^{-1} g_1^{\frac{1}{2}} g_3^{\frac{1}{2}} g_{12}^{\frac{1}{2}} g_{23}^{\frac{1}{2}} XYZ + g^{-1} g_1^{\frac{3}{2}} g_2 g_3^{\frac{3}{2}} g_{12}^{\frac{1}{2}} g_{23}^{\frac{1}{2}} \\ &= g_1^{\frac{1}{2}} g_3^{\frac{1}{2}} g_{12}^{\frac{1}{2}} g_{23}^{\frac{1}{2}} \left(\frac{XYZ + g_1 g_2 g_3}{g} \right), \\ \frac{1}{(g'_x)^2} \sum_{\sigma \in L'_7} w_{\text{loc}}(\sigma) &= g_1^{\frac{1}{2}} g_3^{\frac{1}{2}} g_{12}^{\frac{1}{2}} g_{23}^{\frac{1}{2}} g_{123}^{-1} X_1 Y_2 Z_3 + g_1^{\frac{1}{2}} g_3^{\frac{1}{2}} g_{12}^{\frac{3}{2}} g_{13}^{\frac{3}{2}} g_{123}^{-1} \\ &= g_1^{\frac{1}{2}} g_3^{\frac{1}{2}} g_{12}^{\frac{1}{2}} g_{23}^{\frac{1}{2}} \left(\frac{X_1 Y_2 Z_3 + g_{12} g_{13} g_{23}}{g_{123}} \right).\end{aligned}$$

The equality is equivalent to Item 5 of Proposition 1.

B Full Kashaev parametrization of free-fermionic $C_2^{(1)}$ loops

Let G be a planar quadrangulation with a boundary, V its set of vertices, F its set of internal faces. Then G is necessarily bipartite; we fix a bipartite coloring of V into black and white vertices.

A *train track* of G is a path on the dual graph G^* (defined with “half-edges” on the boundary of G , *i.e.* not connected at the external face), such that whenever it enters a face it exits on the opposite edge of that face; see Figure 22. Let T be the set of all train tracks of G .

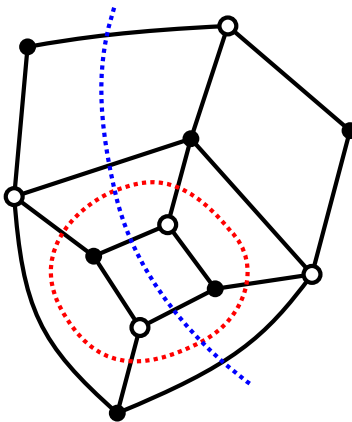


Figure 22: A planar finite quadrangulation with a boundary, and two train tracks.

It is a theorem of Kenyon and Schlenker [31] that a quadrangulation is a lozenge graph *iff* no train track $t \in T$ is a loop or crosses itself, and two distinct train tracks $t, t' \in T$ cross at most once. For instance the quadrangulation of Figure 22 cannot be made of non-degenerate rhombi.

Here we show that on a slightly more general class of quadrangulations, an application is surjective. This linear application will be needed to construct a parametrization such as (17).

Lemma 7. *If G is a connected planar finite quadrangulation with a boundary, such that no train track is a loop, then the mapping*

$$\begin{aligned} \Phi : \mathbb{R}^V &\rightarrow \mathbb{R}^F \\ (h_v)_{v \in V} &\mapsto (h_x + h_y - h_u - h_v) \end{aligned}$$

$f \in F, f = x \begin{array}{c} u \\ \circ \\ y \\ v \end{array}$

is surjective.

Proof. Because of the rank-nullity theorem, it is sufficient to prove that the dimension of $\ker(\Phi)$ is $|V| - |F|$.

Let h be a vector in $\ker \Phi$, and let $t \in T$. We chose an orientation of t . Whenever t crosses a face $f = x \begin{array}{c} u \\ \circ \\ y \\ v \end{array}$, for instance with x, u on its left and y, v on its right, we have $h_x - h_v = h_u - h_y$. This means that the quantity given by the value of h on the right minus its value on the left of an edge crossed by t is constant along t . Let $\alpha_t(h)$ be this value.

If we fix an orientation of every train track and a base vertex x_0 , we thus get a linear transformation from $\ker(\Phi)$ to $\mathbb{C}^{|T|+1}$ by associating $(h_{x_0}, (\alpha_t(h))_{t \in T})$ to h . It is easy to see that this transformation is injective: if the family is null then $h_{x_0} = 0$ and similarly for its neighbors using the train tracks adjacent to x_0 , etc.

Conversely, if we fix values $(\alpha_t)_{t \in T}$ and a h_{x_0} , we can to reconstruct a vector h in the kernel of Φ associated to these values: starting from x_0 , define h on its neighbors using the values α_t associated to train tracks adjacent to x_0 , then on their neighbors, etc. The orientation of train tracks guaranties that these choices are coherent, and the fact that α_t is constant along t is equivalent to $\Phi(h)$ being 0 on every face crossed by t .

Thus $\ker(\Phi)$ has dimension $|T| + 1$.

Let E_{ext} be the set of edges adjacent to the external face, and $E_{\text{int}} = E \setminus E_{\text{ext}}$. Since the train tracks never loop, the set of train tracks define a coupling of external edges so

$$2|T| = |E_{\text{ext}}|. \quad (29)$$

Since every internal face is a quadrangle, we have

$$4|F| = 2|E_{\text{int}}| + |E_{\text{ext}}|. \quad (30)$$

Finally we have Euler's formula:

$$|V| - |E| + |F| = 1. \quad (31)$$

Combining (29), (30), (31) and $|E| = |E_{\text{int}}| + |E_{\text{ext}}|$ easily gives

$$|T| + 1 = |V| - |F| \quad (32)$$

so $\dim(\ker \Phi) = |V| - |F|$ as needed. \square

Now we can go back to the proof that parametrization (17) exists for any free-fermionic loop model on a graph G that satisfies the assumption of Lemma 7.

On every face f we have a set of positive weights w_1^f, \dots, w_5^f that satisfy (6). Let us define $\kappa_f = w_5^f$ and $R_f = \left(\frac{w_1^f}{\kappa_f}\right)^2$. We get:

$$\begin{cases} w_1^f = \kappa_f \sqrt{R_f} \\ w_2^f = \kappa_f \sqrt{\frac{1}{R_f}} \\ w_3^f = \kappa_f \sqrt{1 + R_f} \\ w_4^f = \kappa_f \sqrt{1 + \frac{1}{R_f}} \\ w_5^f = \kappa_f. \end{cases} \quad (33)$$

By Lemma 7, there is a function $h : V \rightarrow \mathbb{R}$ such that on every face $f = x \begin{array}{c} \bullet \\ \circ \\ \bullet \end{array} \begin{array}{c} u \\ \bullet \\ v \end{array} y$,

$$\log(R_f) = h_x + h_y - h_u - h_v.$$

If we set $g_x = e^{h_x}$, we get

$$R_f = \frac{g_x g_y}{g_u g_v}$$

and (33) becomes

$$\begin{cases} w_1^f = \kappa_f \sqrt{\frac{g_x g_y}{g_u g_v}} \\ w_2^f = \kappa_f \sqrt{\frac{g_u g_v}{g_x g_y}} \\ w_3^f = \kappa_f \sqrt{\frac{g_x g_y + g_u g_v}{g_u g_v}} \\ w_4^f = \kappa_f \sqrt{\frac{g_x g_y + g_u g_v}{g_x g_y}} \\ w_5^f = \kappa_f. \end{cases} \quad (34)$$

Multiplying all weights at a face by a same constant doesn't change the relative weights of loop configurations. Here, if we multiply all weights by $\frac{\sqrt{g_x g_y g_u g_v}}{\kappa_f}$, we get the parametrization (17).

Remark 4. *One can prove in exactly the same way that Kashaev’s parametrization of the Ising model [24] is possible whenever the underlying quadrangulation satisfies the assumption of Lemma 7. For instance, the Ising model on any finite isoradial graph admits a Kashaev parametrization.*

References

- [1] M. Assis. The 16-vertex model and its even and odd 8-vertex subcases on the square lattice. arXiv:1702.02110, 2017.
- [2] Y. Baryshnikov and R. Pemantle. Asymptotics of multivariate sequences, part III: Quadratic points. *Advances in Mathematics*, 228(6):3127 – 3206, 2011.
- [3] V. V. Bazhanov. Trigonometric Solution of Triangle Equations and Classical Lie Algebras. *Phys. Lett.*, B159:321–324, 1985.
- [4] C. Boutillier and B. de Tilière. Height representation of XOR-Ising loops via bipartite dimers. *Electron. J. Probab.*, 19:33 pp., 2014.
- [5] G. D. Carroll and D. Speyer. The cube recurrence. *Electr. J. Comb.*, 11(1), 2004.
- [6] D. Cimasoni and N. Reshetikhin. Dimers on surface graphs and spin structures. I. *Communications in Mathematical Physics*, 275(1):187–208, 2007.
- [7] H. Cohn, R. Kenyon, and J. Propp. A variational principle for domino tilings. *Journal of the American Mathematical Society*, 14(2):297–346, 2001.
- [8] J. de Gier, A. Lee, and J. Rasmussen. Discrete holomorphicity and integrability in loop models with open boundaries. *J. Stat. Mech.*, 1302:P02029, 2013.
- [9] B. de Tilière. Quadri-tilings of the plane. *Probability Theory and Related Fields*, 137(3):487–518, Mar 2007.
- [10] P. Di Francesco, P. Mathieu, and D. Senechal. *Conformal Field Theory*. Graduate Texts in Contemporary Physics. Springer-Verlag, New York, 1997.
- [11] P. Di Francesco and R. Soto-Garrido. Arctic curves of the octahedron equation. *Journal of Physics A: Mathematical and Theoretical*, 47(28):285204, 2014.
- [12] C. L. Dodgson. Condensation of determinants, being a new and brief method for computing their arithmetical values. *Proceedings of the Royal Society of London*, 15:150–155, 1866.
- [13] J. Dubédat. Exact bosonization of the Ising model. arXiv:1112.4399, Dec 2011.
- [14] C. Fan and F. Y. Wu. Ising model with second-neighbor interaction. I. Some exact results and an approximate solution. *Phys. Rev.*, 179:560–569, Mar 1969.
- [15] C. Fan and F. Y. Wu. General lattice model of phase transitions. *Phys. Rev. B*, 2:723–733, Aug 1970.
- [16] M. E. Fisher. Statistical mechanics of dimers on a plane lattice. *Phys. Rev.*, 124:1664–1672, Dec 1961.
- [17] S. Fomin and A. Zelevinsky. Cluster algebras. I. Foundations. *J. Amer. Math. Soc.*, 15(2):497–529 (electronic), 2002.
- [18] S. Fomin and A. Zelevinsky. Cluster algebras. II. Finite type classification. *Invent. Math.*, 154(1):63–121, 2003.
- [19] T. George. Limit shapes for cube groves with periodic conductances. arXiv:1711.00790, Nov 2017.

- [20] C. A. Hurst. New approach to the Ising problem. *Journal of Mathematical Physics*, 7(2):305–310, 1966.
- [21] Y. Ikhlef and J. Cardy. Discretely holomorphic parafermions and integrable loop models. *Journal of Physics A: Mathematical and Theoretical*, 42(10):102001, 2009.
- [22] J. L. Jacobsen and J. Kondev. Conformal field theory of the Flory model of polymer melting. *Physical Review E : Statistical, Nonlinear, and Soft Matter Physics*, 69:066108, 2004.
- [23] M. Jimbo. Quantum R matrix for the generalized Toda system. *Comm. Math. Phys.*, 102(4):537–547, 1986.
- [24] R. M. Kashaev. On discrete three-dimensional equations associated with the local Yang-Baxter relation. *Letters in Mathematical Physics*, 38(4):389–397, 1996.
- [25] P. W. Kasteleyn. Graph theory and crystal physics. In H. Frank, editor, *Graph theory and theoretical physics*, pages 43–110. Academic P London, New York, 1967.
- [26] R. Kenyon. Local statistics of lattice dimers. *Annales de l'Institut Henri Poincaré (B) Probability and Statistics*, 33(5):591 – 618, 1997.
- [27] R. Kenyon. The Laplacian and Dirac operators on critical planar graphs. *Inventiones mathematicae*, 150(2):409–439, 2002.
- [28] R. Kenyon, A. Okounkov, and S. Sheffield. Dimers and amoebae. *Ann. of Math. (2)*, 163(3):1019–1056, 2006.
- [29] R. Kenyon and R. Pemantle. Double-dimers, the Ising model and the hexahedron recurrence. *Journal of Combinatorial Theory, Series A*, 137:27 – 63, 2016.
- [30] R. Kenyon, J. Propp, and D. Wilson. Trees and matchings. *The Electronic Journal of Combinatorics [electronic only]*, 7:Research paper R25, 34 p., 2000.
- [31] R. Kenyon and J.-M. Schlenker. Rhombic embeddings of planar quad-graphs. *Transactions of the American Mathematical Society*, 357(9):3443–3458, 2005.
- [32] R. Pemantle and M. C. Wilson. *Analytic Combinatorics in Several Variables*. Cambridge University Press, New York, NY, USA, 2013.
- [33] T. K. Petersen and D. Speyer. An arctic circle theorem for groves. *Journal of Combinatorial Theory, Series A*, 111(1):137 – 164, 2005.
- [34] J. Propp. The Many Faces of Alternating-Sign Matrices. In *DMTCS Proceedings vol. AA, Discrete Models: Combinatorics, Computation, and Geometry (DM-CCG 2001)*, pages 43–58, 2001.
- [35] D. E. Speyer. Perfect matchings and the octahedron recurrence. *Journal of Algebraic Combinatorics*, 25(3):309–348, 2007.
- [36] S. O. Warnaar and B. Nienhuis. Solvable lattice models labelled by Dynkin diagrams. *Journal of Physics A: Mathematical and General*, 26(10):2301, 1993.
- [37] F. Wu and K. Lin. Staggered ice-rule vertex model—the pfaffian solution. *Physical Review B*, 12(1):419, 1975.